X-RAY STRUCTURE ANALYSIS OF CRAB STRIATED MUSCLE

by

Keiichi Namba

Department of Biophysical Engineering

Faculty of Engineering Science

Osaka University

March 1980

PREFACE

The sliding theory for contraction of striated muscle was proposed as early as in 1954 (Huxley & Niedergerke, 1954; Huxley & Hanson, 1954), but still details are not known of structure of muscles. X-ray diffraction technique has more advantage than electron microscopy in studying muscle structure since it can be applied to the living muscle. Also X-ray diffraction pattern of muscle consists of many clear layer-line reflections which should contain good information on muscle structure. Therefore, a key point in studying muscle structure has been how to extract information from the diffraction pattern. One of the aims of this thesis is to propose an analytical method for this purpose. Another is to report results of the structure analysis of the rigor striated muscle of marine crab, *Portunus trituberculatus*, which has been derived with a help of the proposed method.

This thesis consists of two chapters. Chapter I describes the equatorial X-ray analysis made with a help of electron microscopy and the obtained projection of myofibril structure along the fibre axis. Chapter II describes a new method proposed to analyse X-ray layer-line reflections and the three-dimensional structure of the rigor complex of the thin filament determined with the method.

The author wishes to express his sincere thanks to Prof. T. Mitsui and Dr. K. Wakabayashi for their advices, discussion and encouragement during the course of this study. He is grateful also to Prof. F. Oosawa and Dr. T. Yanagida for their advices in the beginning of this study, to Dr. T. Ueki and Mr. M. Kataoka for their helpful discussion on the structure analysis, and to other members in this biophysics laboratory for their helps offered during this study. Thanks are due to Dr. B. M. Millman (Univ. of Guelph, Canada) for his criticism on an earlier draft of Chapter I, Dr. K. C. Holmes (Max Planck Institute, Germany) for supplying a preprint on the insect flight muscle and Dr. E. J. O'Brien (King's College, England) for helpful discussion on Chapter II.

Mr. K. Harajima and other members of Suma Aquarium supplied us living crabs. Prof. R. Suzuki of this department provided us the space for keeping crabs. Their kind arrangements have made the study possible.

CONTENTS

SYNOPSIS 1

INTRODUCTION 3

CHAPTER I X-RAY EQUATORIAL ANALYSIS OF THE CROSS-SECTIONAL STRUCTURE IN THE RIGOR STATE 11

Summary 12

I-1 Introduction 13

I-2 Materials & Methods 16

I-3 Results 20

I-4 Discussions 36

Appendix 44

CHAPTER II X-RAY STRUCTURE ANALYSIS OF THE THIN FILAMENT IN THE RIGOR STATE 48

Summary 49

II-1 Introduction 51

II-2 Materials & Methods 53

II-3 Experimental Results 55

II-4 Structure Analysis 62

II-5 Discussions 87

REFERENCE 100

SYNOPSIS

Results obtained by the studies described in this thesis may summarized as follows.

1. In the striated muscle of crab, *Portunus trituberculatus*, myofilaments are arranged in the hexagonal lattice of lattice constant 63nm ± 1nm.
2. Number of the thin filaments is 6 in one unit cell.
3. The triangle formed by three thick filaments contains a reversed smaller triangle formed by three thin filaments.
4. The electron micrographs of isolated thick filaments gave a hollow core in the central part of the filament. Fourier synthesis was made with X-ray equatorial data referring to this structure, resulting in cylindrical thick filament backbone.
5. Diameters of the thick filament backbone and its hollow core were estimated as 19.6nm and 6.0nm, respectively with X-ray equatorial data.
6. The electron density projected along the filament axis is greater in the thick filament backbone than in the thin filament, indicating that packing of the protein molecules are denser in the thick filament than in the thin filament.
7. There is no appreciable change in the stucture of the thick filament backbone when the relaxed muscle turns into rigor.
8. Comparison of our results with those of Yagi & Matsubara

(1977) suggested that myosin heads are present in the region around 10nm to 20nm in radius from the centre of the thick filament in the relaxed state.

9. The period of the myosin heads projected onto the axis of the thick filament is 14.5nm in the relaxed state.

10. The period of the thin filament is 76.5nm and F-actin have 28 subunits in 13 turns of genetic helix in both the rigor and the relaxed states.

11. The troponin molecules sit with their centres of gravity at roughly the same z coordinates as the 1, 1' and 8, 8' (or 5', 6 and 12', 13) actin monomers when the actin monomers are numbered as 1 ∿ 14 along one strand of the long-pitch helix and 1' ∿ 14' along the other, 1' being neighboured by 1 and 2. Their r coordinate is 6.5nm.

12. Very approximated shape of troponin molecule is an elongated rod 4.0nm wide and 9.5nm long along the filament axis.

13. The S1 are bound to the 3, 3', 4, 4' and 10, 10', 11, 11' actin monomers in the rigor state.

14. The centre of gravity of bound S1 sits at r coordinate of about 2.8nm in the rigor state.

15. Several theorems are presented concerning the difference cylindrically symmetrical Patterson function, which make the function useful in structure analysis of the crab muscle.

INTRODUCTION

Muscle, especially a striated muscle, is the most developed motive organella. A fundamental structural unit of a striated muscle is called sarcomere, and a contractile system consisting of thick and thin filaments has a highly ordered structure in sarcomere. There are four main proteins in the contractile system of vertebrate striated muscle: myosin, actin, tropomyosin and troponin. The thick filament is consisted of myosin, and the thin filament is consisted of actin, tropomyosin and troponin. In invertebrate muscles, a further protein paramyosin is present in the thick filament. There are several constituent proteins except for these. They form the contractile system in a specific arrangement and exert their own function through interaction with each other in muscle contraction.

Historically, physiological studies on muscle such as tension development, velocity of shortening, heat production and energetics of contraction proceeded without reference to the details of structure. Subsequently, several discoveries in muscle biochemistry were made and the actomyosin-ATP system was established as a source of chemical energy of muscle contraction (Szent-Györgyi, 1951). In 1954, very important observations on the structure of the striated muscle were done at the same time by A. F. Huxley & Niedergerke (1954) with the optical microscope

and H. E. Huxley & Hanson (1954) with the electron microscope, and the sliding-filament model on contraction of striated muscles was proposed by them. Physiological data on muscle contraction obtained so far have been explained phenomenologically by the sliding-filament model (Huxley, 1957; Podolsky, Nolan & Zavelar, 1969; Huxley & Simmons, 1972). In the 1960's, troponin which is a calcium-sensitive protein was discovered and the troponin-tropomyosin system was found to have a regulatory function of muscle contraction (Ebashi & Endo, 1968). In the 1970's, the reaction schemes for ATP hydrolysis in the actomyosin system were proposed (Tonomura, 1972; Taylor, 1972). Over past 30 years, the physical and chemical processes of muscle contraction on a molecular level have been extensively studied by various techniques and a great deal of evidence has been given to the mechanism of muscle contraction. It has been now possible to understand systematically the mechanism of contraction of striated muscle on a molecular level.

According to the recent sliding-filament model, the active sliding force is developed by the heads of myosin molecules which attach to the thin filaments and exert a longitudinal force. These myosin heads called the crossbridges, act in a cyclical manner and produce the relative sliding of the thick and thin filaments for a distance about 8nm, and then they release and re-attach to the thin filaments at another point. The cycle recurs

and a continuous motion of the filaments is produced. The cycling of the crossbridges can be closely related with the steps in the reaction schemes for ATP hydrolysis in the actomyosin system. Therefore, the complex of the thin filament and the attached myosin heads is important part of the generation of sliding force and thus the basic contractile unit. The attachment of the myosin heads to actin is regurated by the troponin-tropomyosin system depending on the concentration of calcium ions.

However, it is not known that how the force generating mechanism requires the conformational changes of the actomyosin complex and how the regulatory proteins control the interaction of actin and myosin head. To understand the crossbridge mechanism we need to visualize the dynamical behaviour of actomyosin complex on a molecular and submolecular levels. Unfortunately, there is no technique which allow us to visualize it at present, but it has become possible to observe the way which the myosin heads remain attached under certain circumstances. Negative-staining techniques in the electron microscope have shown the arrow-heads structure of the complex of the thin filament and the attached myosin heads (e.g., Huxley, 1969). More recent image reconstruction techniques of the electron micrographs have visualized the structures of the reconstituted actomyosin complexes (Moore, Huxley & DeRosier, 1970; Spudich, Huxley & Finch, 1972). The

possible structural changes of the regulatory proteins in the thin filament have been also shown by this method (Wakabayashi et al., 1975). On the other hand, X-ray diffraction technique has been used to determine the structural parameters of myofilaments *in vivo*. Since the X-ray source was not yet strong enough to detect active changes during muscle contraction, the X-ray diffraction was limitted to the studies of the static structures of muscle. X-ray diffraction has shown that a large change of diffraction patterns occurs when the muscle changes the states. This change of diffraction patterns has been explained by the mass transfer from the thick to the thin filaments accompanied by contraction. It has been attributed to the movement of myosin heads (Huxley & Brown, 1967; Huxley, 1968; Haselgrove & Huxley, 1973). Recently, use of much more powerful X-ray source and development of skillful detection procedures of X-ray have been attempted to make dynamical X-ray diffraction for studies of dynamical behaviour of the crossbridges, and the crossbridge mechanism has been discussed on the basis of changes of diffraction patterns.

In order to interpret the dynamical change of the diffraction patterns, detailed knowledge of the structure of the muscle in the static state will be essentially necessary. However, knowledges of the structure of the muscle so far obtained was insufficient, since interpretations

of diffraction patterns have remained the qualitative ones, especially for the axial diffraction patterns. Until now there has been no adequate description of the structure of rigor muscle which is one of the forms of the actomyosin complex, and furthermore no general method of analysis of the diffraction patterns has been given. The muscle which is assembly of many myofibrils is not a single crystal. Myofibril is a heterogeneous system consisting of thick and thin filaments with different structural periodicities. In each myofibril, these myofilaments are arranged in a two-dimensional hexagonal lattice and sometimes form the three-dimensional lattice with certain particular disorders, but is generally incomplete. Therefore the equatorial diffraction pattern consists of Bragg reflections due to the lattice arrangement of filaments and the axial diffraction pattern consists of continuous layer-line reflections in which the lattice sampling appears partially or incompletely. For these reasons, application of the methods used in the crystallographic analysis has been accompanied by many practical difficulties and thus the quantitative analysis has not been made. It is needed to develop a way to overcome such difficulties and to derive the structural informations by the quantitative analysis of the diffraction patterns. Such an approach has been recently made for insect flight muscle by Barrington Leigh et al. (1977) and Holmes, Tregear &

Barrington Leigh (1979). We have proposed another way of such approach and applied it to structure analysis of the thin filament of the rigor muscle of marine crab, *Portunus trituberculatus*. Fig.1 shows the crab. Fig.2 indicates the portion of muscle in swimming leg of the crab which was used for our studies.

We have been interested in the structure of the thin filaments, since the thin filament is the stage of the interaction between actin and myosin heads and the regulation of contraction by the troponin-tropomyosin system. A crab muscle contains more and longer thin filaments than vertebrate muscles. X-ray diffraction pattern from the crab muscle has shown many sharp layer-line reflections due to the thin filaments and a few weak reflections due to the thick filaments. No lattice sampling effect has been present on any layer lines except on the equator, being much favorable for the analysis of the structure of the thin filaments.

The thesis contains two chapters. In Chapter I, the equatorial X-ray analysis is described and the basic structure of the cross-section of myofibril in the crab leg muscle is presented before going to the main analysis. In Chapter II, the layer-line diffraction analysis based on a modified Patterson function is described and the structure of the rigor complex of the thin filament is presented.

Fig.1. *Portunus trituberculatus*

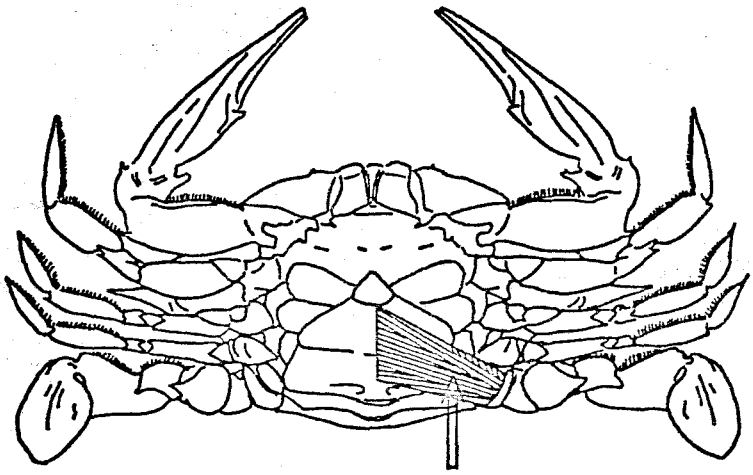

Fig.2. The portion (arrowed) of muscle used in the study

CHAPTER I

X-RAY EQUATORIAL ANALYSIS OF THE CROSS-SECTIONAL STRUCTURE IN THE RIGOR STATE

Summary

The cross-sectional structure of a striated muscle of the marine crab, *Portunus trituberculatus*, in the rigor state was studied by electron microscopy and X-ray diffraction.

Electron micrographs of transverse sections showed that the thick filaments are arranged in a hexagonal lattice and the unit cell contains 6 thin filaments and one thick filament. A non-staining core in the centre of the thick filament which has been observed in the sectioned muscles was identified as a hollow core by a negative-staining method.

X-ray equatorial diffraction patterns from a rigor muscle showed nine distinct reflections which were indexed for a hexagonal lattice having a lattice constant of 63nm ± 1nm. Using these reflections, the electron density distribution of the axial projection was determined at a resolution of 7nm by the Fourier synthesis with the help of the electron microscopy. This gave a diameter for the thin filament of 12.4nm and for the thick filament of 19.6nm. The thick filament had a low electron density core 6.0nm in diameter. The electron densities of the filaments in the projection were determined on an absolute scale, showing that the electron density was greater in the thick filament. Our results for the rigor muscle were compared with those for the relaxed muscle of another species of crab by Yagi & Matsubara (1977).

I-1. Introduction

The myofibrils of invertebrate muscles have cross-striated similar to those of vertebrate skeletal muscles (Reedy, 1968; Smith, 1972). One of the main structural differences among those muscles is in the arrangement of the thin and thick filaments in the myofibrils. Electron micrographs of transverse sections of striated muscles have shown a hexagonal lattice of the thick filaments (Huxley, 1957). In vertebrate skeletal muscles, each thick filament is surrounded by six thin filaments which occupy the trigonal positions. There are two thin filaments per unit cell and each is shared by three thick filaments (Huxley, 1957; Smith, 1972). In insect flight muscles, the thin filaments occupy the two-fold positions between two thick filamtns and there are three thin filaments per unit cell. Each thin filament is shared by two thick filaments (Reedy, 1968; Smith, 1972). On the other hand, in many crustacean muscles, the content of thin filaments in the myofibril is further increased and thus the arrangement of the thin filaments differs from those of vertebrate skeletal and insect flight muscles (Smith, 1972; Pringle, 1972). It has been reported that there exist nine to twelve thin filaments around each thick filament (Smith, 1972). Another structural feature of many invertebrate muscles is that the thick filament has a diameter larger than

vertebrate skeletal muscles and contains paramyosin. Electron micrographs in the cross section of these muscles show a non-staining core in the centre of the thick filament.

X-ray equatorial studies have been done on vertebrate skeletal and insect flight muscles and demonstrated the change of the electron density distribution in the cross section referring to muscle contraction (Huxley, 1968; Haselgrove & Huxley, 1973; Barrington Leigh & Rosenbaum, 1976). Though it has been pointed out that the change corresponds to the movement of myosin heads (Huxley, 1968), positions of myosin heads have not been clealy revealed in the relaxed state or in contraction.

We have studied on the striated muscle of crab, *Portunus trituberculatus*, by electron microscopy and X-ray diffraction to determine the cross-sectional structure and to demonstrate the changes of electron density distribution in the rigor and relaxed states (Namba & Wakabayashi, The 16th Ann. Meeting of Biophys. Soc. Japan, Abstr. 29-C-26 (1977)). The crab leg muscle used in our studies is cross-striated, with band patterns similar to those in vertebrate skeletal muscles. Its sarcomere length (5.5μm) is longer than that of vertebrate skeletal muscles. Although sufficient biochemical and physiological data are not available at present, the thin filament contains the proteins, actin, tropomyosin and troponin, and the thick filament contains the proteins, myosin and paramyosin

(Maéda, Matsubara & Yagi, 1979; Wakabayashi, Ichikawa & Namba, unpublished results).

Recently, Yagi & Matsubara (1977) reported X-ray equatorial analyses on the leg muscle of another species of crab, *Plagusia dentipes*, and the abdominal muscle of crayfish, *Cambarus clarkii*, and proposed a model for the thick filament with a hollow core. They have analysed the diffraction patterns from living relaxed muscles and derived the electron density distribution of the axial projection for the relaxed muscles. They also recorded rigor patterns but did not analyse these in detail, since they could not obtain good diffraction patterns with sharp reflections as in the relaxed patterns. In contrast to them, we have obtained so far the good diffraction patterns for the rigor muscle of crab (*Portunus trituberculatus*) and determined the cross-sectional structure for the rigor muscle by the Fourier synthesis with the help of the electron microscopy. The same conclusion was derived for the thick filament with the hollow core, but the details differ slightly from their results. In this Chapter, our results for the rigor muscle is described as a complement of the work of Yagi & Matsubara (1977) and discussed in conjunction with their results for the relaxed muscle of crab (*Plagusia dentipes*).

I-2. Materials & Methods

(a) Specimens

Striated muscle from the swimming leg of the marine crab, *Portunus trituberculatus*, was used for this study.

Fibres were dissected from the white leg muscles. Glycerination of the fibres was promoted at the sarcomere length of about 5.5μm by immersing in 50% glycerol-water containing 1mM EGTA buffered with 10mM Tris maleate (pH 7.0) at -15°C for more than two weeks (Yanagida, Taniguchi & Oosawa, 1974). A single fibre or a bundle containing 2 ∿ 5 single fibres was immersed in rigor or relaxing solution and used as specimens for electron microscopy and X-ray diffraction. The thickness of a single fibre was 300μm. The composition of the rigor solution was 100mM KCl, 10mM $MgCl_2$, 1mM EGTA and 10mM histidine-HCl (pH 7.0). Relaxing solution was prepared by adding 10mM Na_2ATP to the rigor solution.

Living relaxed muscles were also used. They were immersed in a cold crab Ringer's solution containing 400mM NaCl, 24mM KCl, 20mM $CaCl_2$, 16mM $MgCl_2$, 0.2mM $NaHCO_3$ and 100mM glucose (Yanagida et al., 1974).

The sarcomere length of the muscle was measured from light diffraction patterns using a He-Ne gas laser (NEC, GLG-2026, Tokyo). It was determined as 5.5μm ± 0.3μm. Observation with a phase contrast microscope (Olympus Model FHT-533) confirmed that the length of the A band occupied

70 ∿ 80% of the sarcomere length of 5.5μm.

(b) Electron microscopy

Sectioned preparation of muscles

Glycerinated fibres were fixed by immersion in 1% glutaraldehyde in 10mM cacodylate buffer (pH 7.0). They were post-fixed in 3% osmium tetraoxide in the same buffer. The fixed fibres were dehydrated through increasing concentrations of ethanol and then propylene oxide. They were embedded in Epon regin. Staining was done with 1% uranyl acetate (pH 7.0) before dehydration by ethanol. Thin transverse and longitudinal sections were cut on a Porter-Blum MT-1 ultramicrotome.

Negatively stained preparation of thick filaments

Filament suspensions from living muscles were prepared by the method of Szent-Györgyi, Cohen & Kendrick-Jones (1971). Filaments were finally suspended in the relaxing solution. A drop of the filament suspension was placed on a carbon-coated specimen grid and the filaments were negatively stained with 3% uranyl acetate.

All specimens were examined in a Hitachi HU-11-S electron microscope. The magnification was calibrated by using Dow polystyrene latex particles.

(c) X-ray diffraction

The fibres were attached tightly to the specimen holder in an acrylic plastic cell. The cell has two thin mylar windows allowing the X-rays pass through. The specimen holder was cooled to 4°C with a Coolnics thermoelectric cooler (Komatsu-Yamato, Tokyo). Cooled rigor or relaxing solution for glycerinated muscles and cooled Ringer's solution for living muscles were circulated in the cell with a peristaltic pump during X-ray exposures.

The X-ray source was a Rigaku-denki microfocus rotating anode generator with a copper target (type RU3HM) operated at 55kV with a tube current of 6mA. The focus size, viewed at an angle of 6°, was approximately 100 × 100μm^2. A mirror-monochromator camera of the type described by Huxley & Brown (1967) was used to obtain low angle diffraction patterns. The curved glass mirror was placed at 20cm from the source and the bent quartz crystal monochromator (3°-cut to $(10\bar{1}1)$) was placed at 7cm from the mirror. A vacuum tube, enclosing most of the X-ray path, was used to eliminate air-scattering. The size of the X-ray focus on the film which contains only $CuK\alpha_1$ radiation (λ=1.5405Å), was about 70 × 150μm^2. Good focus was obtained by monochromator, but the focus by the total reflecting mirror was not so good because of the asymmetric position of symmetric bending mirror. In order to get good spatial resolution in the equatorial direction, the

fibre was set perpendicular to the focusing direction of monochromator. Diffraction patterns were recorded on Fuji medical KX films having a film factor of 1.52. Four films were packed on a film cassette to cover a wide range of intensity. Specimen-to-film distance was determined to be 35.0cm by calibration, using powder pattern of sodium myristate (see International Table for X-ray Crystallography ed. by Kasper & Lonsdale, Vol.III, p.331 (1968)).

(d) X-ray intensity data

The optical density of the film was measured with a densitometer (Nalumi type C, Tokyo). It was converted to the diffraction intensity by a standard scale made by varying exposure time. The intensity curve was obtained as a function of the reciprocal radial coordinate, R ($=2\sin\theta/\lambda$). Background was subtracted from the intensity curve by assuming a monotonic decrease as R increases. Reflections with close spacings were separated by estimating the width of the reflections relative to the direct beam (e.g., see Fig.I-4). Integrated intensity of each Bragg reflection was determined as the area under the peak. Lorentz corrections were applied to the intensities by multiplying each intensity by the appropriate R.

(e) Calculations

Calculations were carried out on a NEAC 2200-MODEL 700 computer at the Computer Centre of Osaka University.

I-3. Results

(a) Electron microscopy

Figs.I-1(a) and (b) show electron micrographs of the transverse and longitudinal section of the crab leg muscle in rigor. The transverse section shows the structure of the overlap region of the thick and thin filaments. Thick filaments are arranged in a hexagonal lattice. The average distance between them is about 60nm, which is close to the value from our X-ray measurements. The positions of the thin filaments do not appear to be as well-defined as those of the thick filaments. This is probably caused by artifacts during preparation of sectioned specimens, since X-ray diffraction patterns have shown sharp Bragg reflections over fairly wide range suggesting the regular array of the filaments in the lattice. Therefore, the number of the thin filaments around a thick filament was counted over large areas of the electron micrographs. The results showed that there exist twelve thin filaments around each thick filament. Careful inspections of the micrographs confirmed that three thin filaments are located in an area surrounded by three thick filaments and that the arrangement of these three thin filaments was in reverse configuration with respect to that of surrounding three thick filaments. This configuration indicates that the ratio of the number of thin-to-thick filaments in the unit cell is 6 (see later, FigI-7(a)). This arrangement of

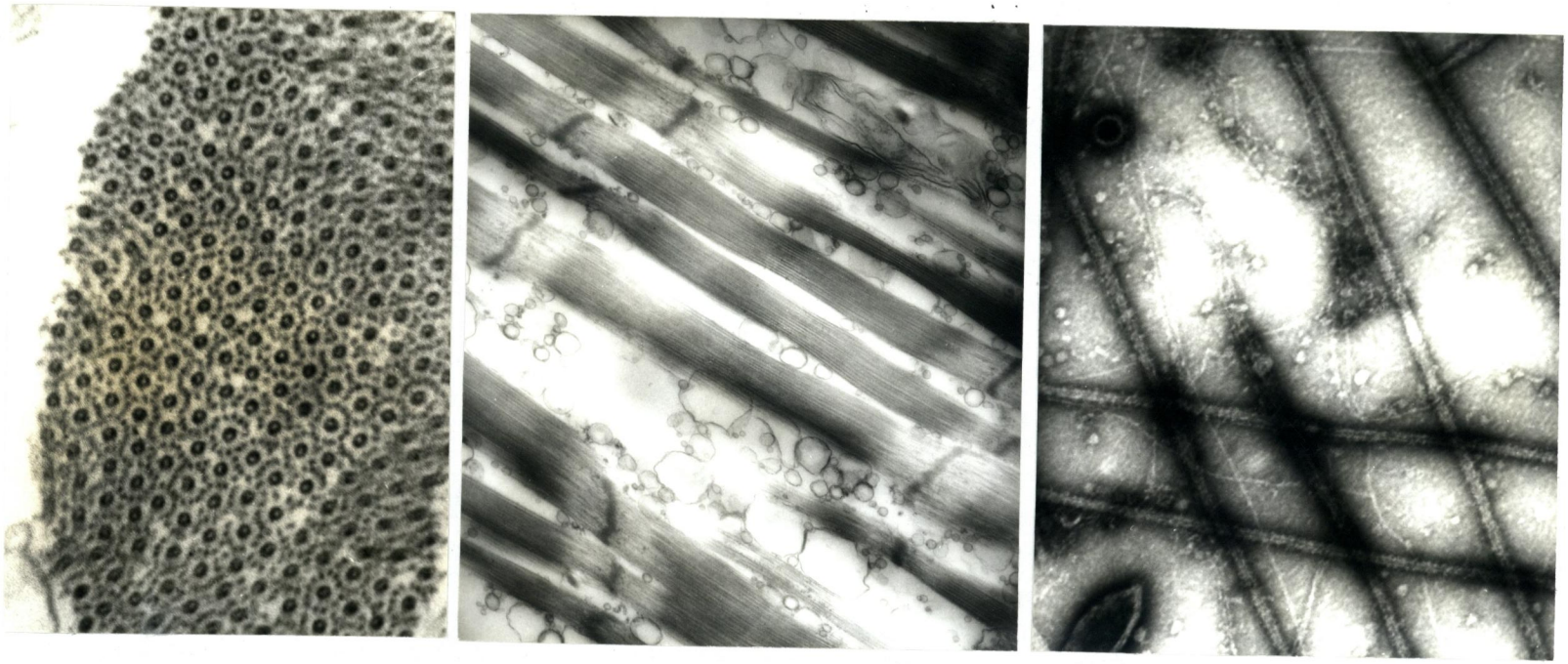

(a) (b) (c)

Fig.I-1. (a) electron micrograph of a transverse section of glycerinated leg muscle of crab (*Portunus trituberculatus*) in rigor. The overlap region of the thick and thin filaments is shown. Scale, 0.1μm. (b) Electron micrograph of a longitudinal section of the same specimen as (a). Scale, 1μm. (c) Electron micrograph of negatively stained isolated thick filaments. Scale, 0.1μm

the thin filaments has been also observed in the electron micrograph of another species of crab muscle (*Plagusia dentipes*) by Maéda (1978).

In our observation, the diameter of the thick filaments was between 20nm to 22nm, which might be larger than vertebrate skeletal muscles and that of the thin filaments was between 7nm to 9nm. But filament diameters are difficult to determine from the electron micrographs, since we do not know the amount of shrinkage of the filaments that might have occurred during preparation.

The characteristic appearance of the thick filament in the electron micrographs (Fig.I-1(a)) has a non-staining core in the centre of the thick filament in the overlap region. The diameter of this core is approximately 7nm. Such a hollow appearance of the thick filaments in cross section has been observed in other muscles which contain paramyosin in the thick filament (e.g., insect flight- Auber & Couteaux, 1963 and Bullard, Hammond & Luke, 1977; scallop- Millman & Bennett, 1976; crayfish- April, Brandt & Elliott, 1971 and Yagi & Matsubara, 1977; crab- Yagi & Matsubara, 1977 and Maéda, 1978). This appearance indicates that no protein occupies the core or that a protein which has different staining properties from myosin is present there. In order to determine whether the non-staining core is hollow or not, the negative staining technique was applied to isolated thick filaments.

Fig.I-1(c) shows an example of the electron micrographs of negatively stained thick filaments. The micrograph reveals the axial dense hollow runs down the centre of the thick filament similar to TMV particles (Brenner & Horne, 1959). This appearance indicates that the stain penetrated into the central portion of the thick filaments and that the non-staining core observed in cross section is a hollow core.

(b) Equatorial X-ray diffraction

X-ray diffraction patterns from crab leg muscle were made at the sarcomere length of 5.5μm. Fig.I-2 shows an equatorial diffraction pattern from a rigor muscle. Nine reflections were observed up to a spacing of about 12nm. Beyond this region, reflections were very diffuse and weak. Curve "a" in Fig.I-3 shows the intensities of the reflections in Fig.I-2. All these reflections were indexed for a hexagonal lattice of lattice constant (defined by $2/\sqrt{3}$ × the spacing of the 1,0 reflection) 63nm ± 1nm as indicated in Fig.I-3. In a relaxed muscle, the diffraction pattern was also observed in the same angular region, but reflections were broad and overlapping because of disorder. In living relaxed muscle, only the first three reflections were recorded because we could not keep the muscle alive long enough to record the reflections in the same range as in the rigor muscle. Curve "b" in Fig.I-3 shows the

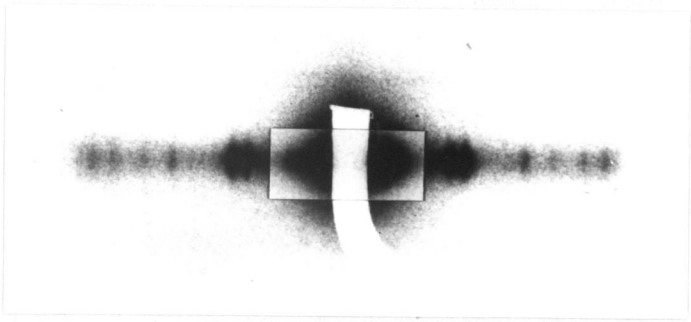

Fig.I-2. Small-angle X-ray equatorial diffraction photograph of the glycerinated leg muscle of the crab (*Portunus trituberculatus*) in rigor. Sarcomere length, 5.5μm ± 0.3μm; Specimen-to-film distance, 35cm; the fibre axis, vertical; exposure time, 70hr.

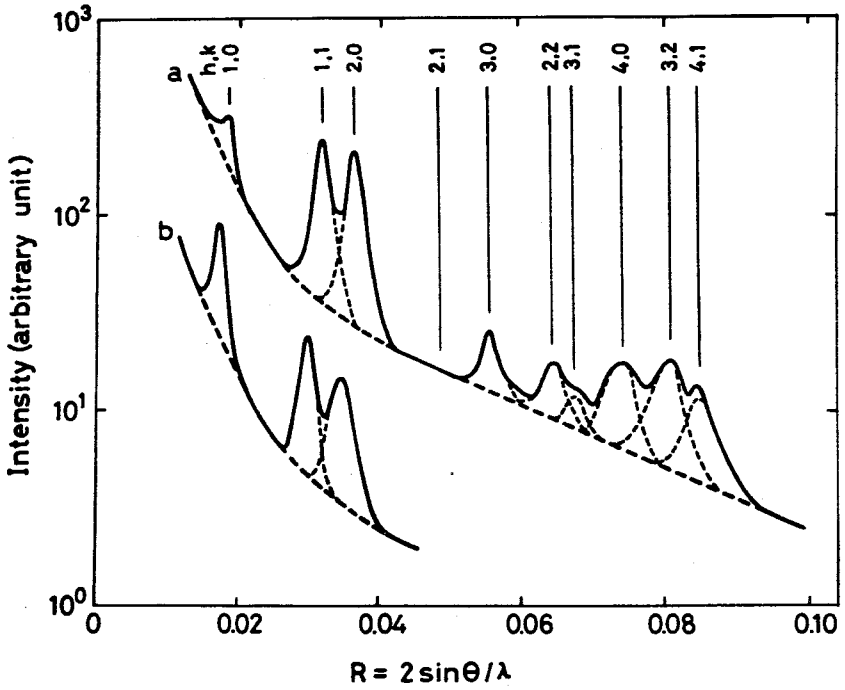

Fig.I-3. Intensities of Fig.I-2 as a function of R(=2sinθ/λ). a, rigor muscle; b, living relaxed muscle. Peaks are indexed with Miller indices (hk) of a hexagonal lattice. Dashed line, the background; thin dashed line, the profile of the reflections (see text).

intensities of these reflections. We have not so far observed additional reflections which seem to come from the thin filament lattice adjacent to or in the Z-line as observed in the vertebrate skeletal muscles (Elliott, Lowy & Millman, 1967). In the crab muscle, these reflections would be very weak in comparison with the observed reflections and also seem to be much more weaker than from the vertebrate skeletal muscles since the sarcomere length fo crab muscle is much longer than that of vertebrate skeletal muscles. Elliott, Lowy & Worthington (1963) suggested that the equatorial Bragg reflections indexed on the hexagonal lattice are caused by the A band. As shown in Fig.I-1(b), overlap region occupies 95% of the A band. Thus, the observed reflections are mostly come from the overlap region.

In both rigor and relaxed muscles, the 1,0, 1,1 and 2,0 reflections were strong and the 1,1 and 2,0 reflections were almost equal in intensity. The intensities of these reflections differ from those observed in vertebrate skeletal muscles where the 2,0 reflection is very weak at the rest length of sarcomere (e.g., Haselgrove, Stewart & Huxley, 1976), and in insect flight muscle where the 1,1 reflection is weak (e.g., Goody et al., 1975). These differences seem to reflect the different arrangement of the thin filaments in the lattice. Millman & Bennett (1976) reported that the same difference was found in

scallop muscle. The intensity ratio of the 1,0 to 1,1 or 1,1 + 2,0 reflections decreased when the crab muscle changed from the relaxed to the rigor state (see Fig.I-3 and also compare with the result of Yagi & Matsubara (1977)). This change is quite similar to that observed in the other muscles (Huxley, 1968; Miller & Tregear, 1972; Millman & Bennett, 1976) and is caused by myosin heads attaching to the thin filaments (Namba et al, 1979). In the present study, diffraction patterns of high quality were obtained only for the rigor muscle and the analysis was made for the rigor muscle. The result will be discussed in context with that of the relaxed muscle of crab (*Plagusia dentipes*) by Yagi & Matsubara (1977).

(c) Electron density distribution in the axial projection

In order to derive the electron density distribution projected along the fibre axis in the rigor muscle, the Fourier synthesis was calculated using the relative intensities of ten reflections to a resolution of 7nm. In Fig.I-3, there exists overlap between peaks of the reflections in the range of $0.06nm^{-1} < R < 0.095nm^{-1}$. As mentioned previously, these reflections were separated by estimating the width of the reflections relative to the direct beam with reasonable accuracy. Small uncertainties in separating them did not cause appreciable changes in the resulting Fourier syntheses. The relative

values of $|F(hk)|$ $(= I(hk)^{1/2})$ of these ten reflections are given in Table I-1. Assuming that the projection of the structure has centre of symmetry, all combinations of phases (0 or π) for the reflections were tried and the two-dimensional Fourier maps were constructed. Among a number of maps obtained, we chose several possible maps on the basis of suggestions from electron micrographs that the electron density of the thin filaments is localized, the number per the unit cell is 6 and the thick filament has a hollow core. Figs.I-4(a) $\sim$ (d) show four maps which are content with the above-mentioned first two criteria. Phases for $|F(hk)|$ used in these four Fourier syntheses are given in Table I-1. All these maps show large areas of high electron density on the corners of the unit cell and smaller areas at positions about 15° around the lattice points from the line joining two neighbouring lattice points. They indicate the electron density distributions of thick and thin filaments, respectively. The maps of Figs.I-4(a) and (b) show the low electron density core in the centre of the thick filaments and thus only these two maps satisfy the above-mentioned last criterion. As the muscle is in the rigor state, the substantial myosin heads are attaching to the thin filaments. Thus the electron density distribution describe their backbone. Figs.I-4(a) and (b) indicate that the thick filament backbone has a hollow core and nearly smooth cylindrical surface.

Table I-1

Comparison of observed amplitudes with calculated amplitudes of h,k reflections

h,k	$\lvert F_{obs}(hk)\rvert$	α_{hk} (a)	(b)	(c)	(d)	$\lvert F_{calc}(hk)\rvert$	$\alpha_{hk,calc}$
1,0	100	0	0	0	0	100	0
1,1	199	0	0	0	0	216	0
2,0	207	0	0	0	0	178	0
2,1	0	0	0	0	0	6	0
1,2	0	0	0	0	0	6	0
3,0	67	π	0	π	π	65	π
2,2	60	π	π	π	0	75	π
3,1	33	0	0	0	0	51	0
1,3	33	0	0	0	0	51	0
4,0	103	π	π	π	π	101	π
3,2	82	π	π	0	0	78	π
2,3	82	π	π	0	0	78	π
4,1	66	π	π	π	π	76	π
1,4	66	π	π	π	π	76	π

$\lvert F_{obs}(hk)\rvert$ were determined as $I(hk)^{1/2}$, where $I(hk)$ are integrated intensities after Lorentz correction. α_{hk} used for the Fourier syntheses of Figs.I-4(a) $\sim$ (c) are given. $\lvert F_{calc}(hk)\rvert$ and $\alpha_{hk,calc}$ are for the best-fit model. All values of $\lvert F(hk)\rvert$ are expressed relative to $\lvert F(10)\rvert$ normalized to 100.

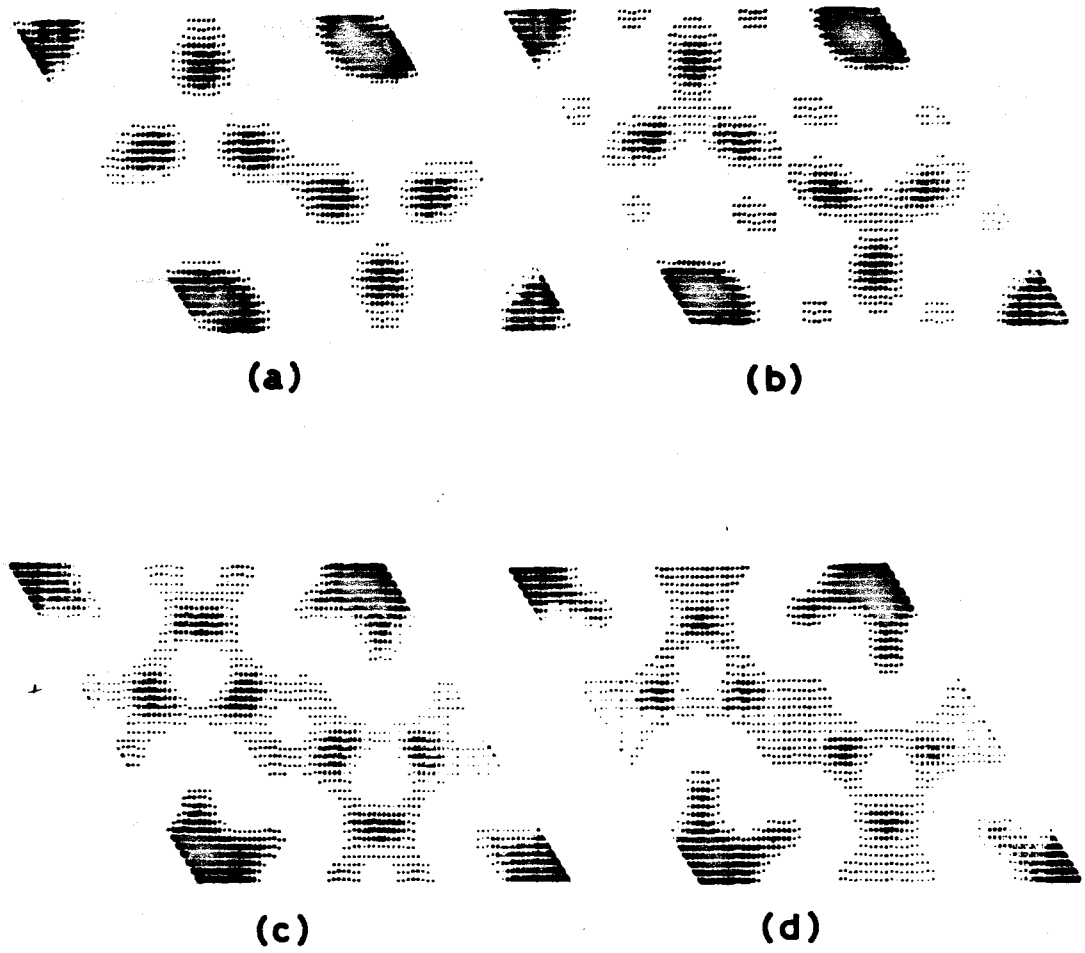

Fig.I-4. Two-dimensional Fourier maps. Four Fourier maps are shown in an arbitrary scale. Phases for the structure amplitudes used in these Fourier syntheses are given in Table I-1. The maps of (a) and (b) show a low electron density core in the centre of the thick filament.

Consequently, we regarded that the maps of Figs.I-4(a) and (b) describe plausible electron density distributions of the cross section of the rigor muscle.

(d) Determination of structural parameters

We tried to determine the electron density on an absolute scale. Several diffraction patterns using the same specimen were measured under the same experimental conditions, but changing the electron density of the solvent in which the muscle fibre was immersed by adding glycerol. We obtained integrated intensities for the 1,1, 2,0, 3,0 and 3,2 reflections after correcting for absorption by the solvent. The relative $|F(hk)|$ of these reflections were plotted against the electron density of the solvent in Fig.I-5. They decreased linearly with increase of the electron density of the solvent, and coincided at a value of $0.4e/\mathring{A}^3$ when extraporated to the abscissa. The other reflections were weak, but changed in intensity similarly to these four reflections. This result indicates that the solvent penetrated into the low electron density core of the thick filament, and that the mean electron density of the constituent proteins of the myofilaments is about $0.4e/\mathring{A}^3$.

In the electron density distributions of Figs.I-4(a) and (b) expressed in an arbitrary scale, the electron density of the outer part of the thick filament was greater

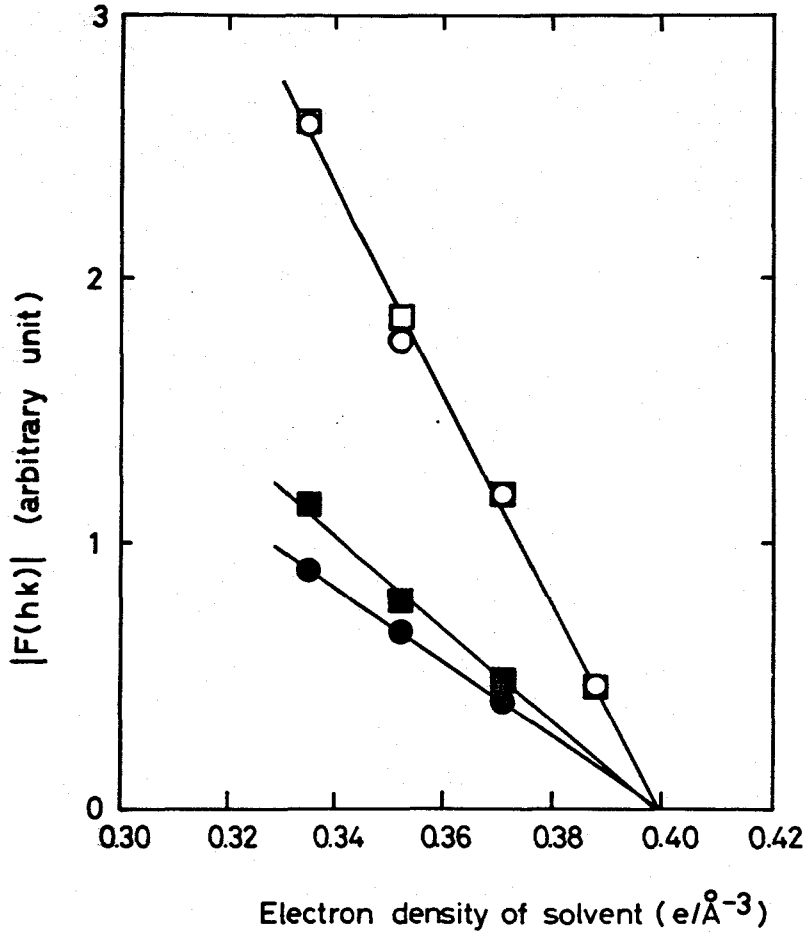

Fig.I-5. Changes of |F(hk)| with the electron density of solvent, which was varied by adding glycerol.
○, |F(11)|; □, |F(20)|; ●, |F(30)|; ■, |F(32)|.

than that of the thin filament. The electron density projected along the fibre axis is the averaged electron density, and would depend on the packing manner of the constituent molecules in the filaments. The layer-line diffraction pattern from the rigor muscle showed many distinct reflections due to the thin filaments and only a few weak reflections due to the thick filaments (Namba et al., 1979), suggesting that the constituent molecules are packed most compactly in the thick filament backbone and are packed loosely in the thin filament. Therefore, we assumed that the maximum electron density of the thick filament in the Fourier maps is equal to the mean electron density, $0.4e/\mathring{A}^3$ (for full discussions, see Appendix). The lowest level in the maps of Figs.I-4(a) and (b) on which ripples were smoothed, was assumed to be the density level, $0.335e/\mathring{A}^3$ of the solvent in between filaments. Figs.I-6(a) and (b) show the electron density distributions along the (1,0) and (1,1) planes of Figs.I-4(a) and (b), described in an absolute scale.

In order to determine structural parameters for the both filaments of the rigor muscle, we derived a step function model approximating the electron density profiles shown in Fig.I-6. To obtain the best-fit step function, we calculated structure amplitudes for the model of the filament lattice shown in Fig.I-7(a). As shown in Fig.I-7(b), variables used in the calculation were the

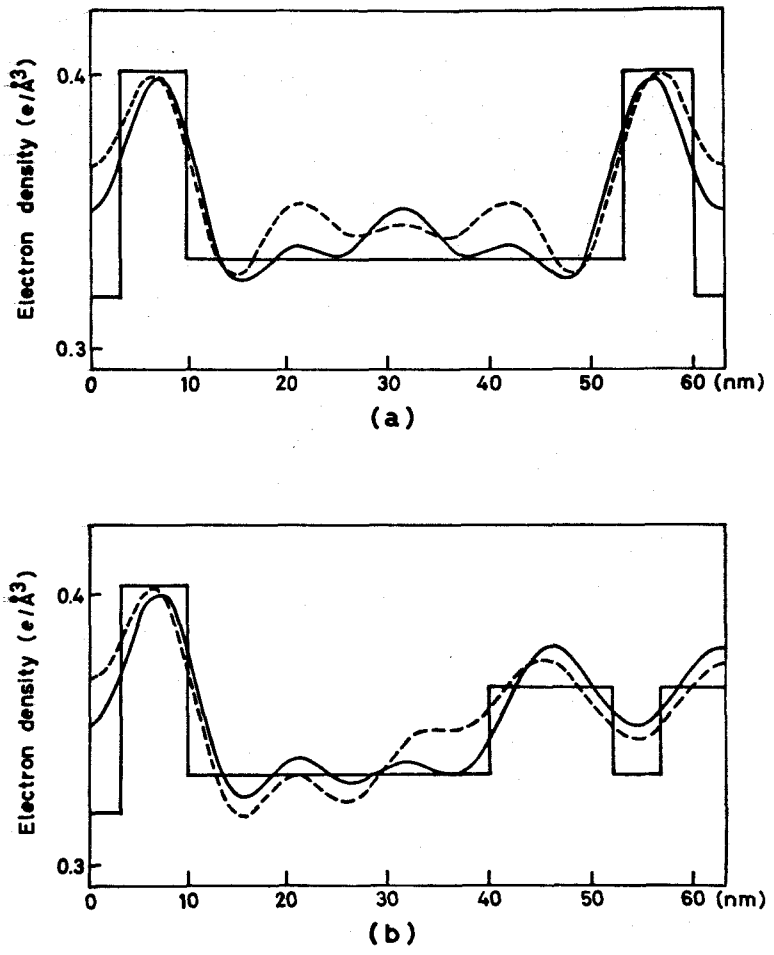

Fig.I-6. Electron density distributions along (a) the (1,0) plane and (b) the (1,1) plane expressed in an absolute scale. Solid line curve corresponds to Fig.I-4(a) and dashed line curve to Fig.I-4(b). The step function of the best-fit model is superimposed.

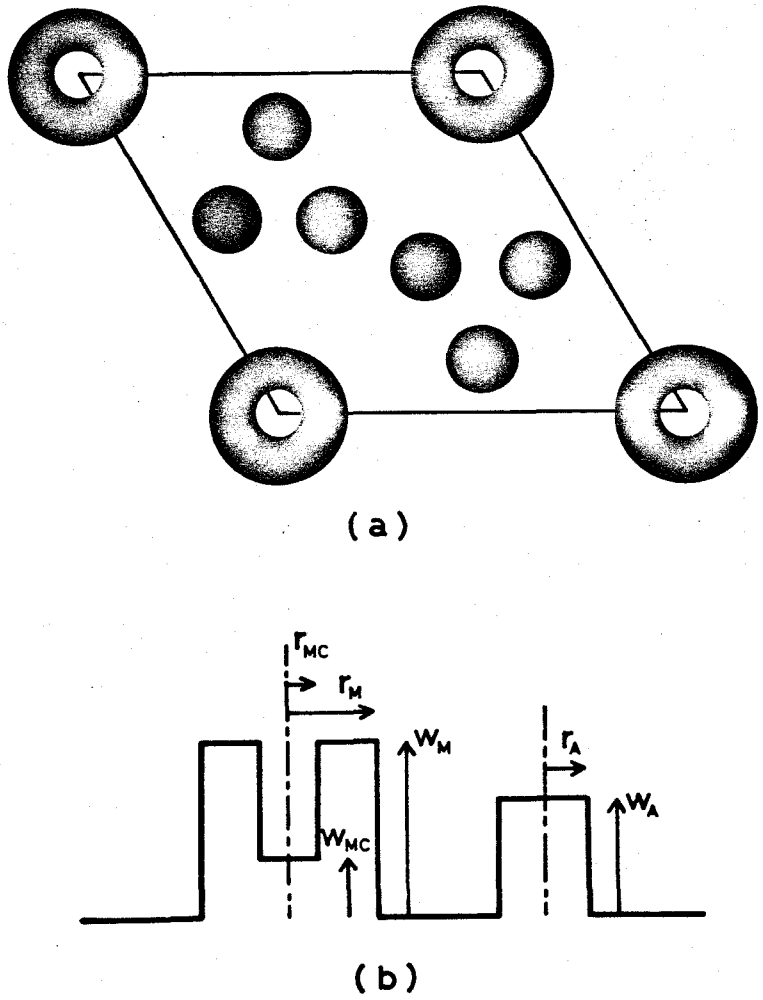

Fig.I-7. Models of the filament lattice in the crab muscle. (a) the structure of the cross-section of one unit cell. The large circle represents the thick filament and the small white circle in it indicates the part where the electron density is lower. The small solid circle, the thin filament. (b) step functions for the electron density profiles of the filaments in a section through the centre. See text for the letters.

radii and weight per unit volume of : the thin filament (r_A, w_A), the thick filament (r_M, w_M), and the thick filament core (r_{MC}, w_{MC}). We determined the model having the minimum value of $R = \sum_{h,k} ||F_{calc}(hk)|-|F_{obs}(hk)|| / \sum_{h,k} |F_{obs}(hk)|$ as the best-fit model. Calculated structure amplitudes and their phases of the best-fit model (R=0.13) are shown in Table I-1. The step functions of the (1,0) and (1,1) planes of this model are depicted in Figs.I-6(a) and (b), superimposed on the experimental profiles. Parameters determined were r_A=6.2nm, r_M=9.8nm, r_{MC}=3.0nm, w_A=0.365e/Å^3, w_M=0.402e/Å^3, w_{MC}=0.322e/Å^3. As shown in Table I-1, phases of the structure amplitudes of this model are the same as for the structure of Fig.I-4(a).

I-4. Discussions

In calculating the Fourier syntheses, we assumed that the projection of the structure has centre of symmetry, so that all phases are 0 or π. The layer-line reflections due to the thick filaments from the relaxed muscle showed very similar appearance to that from the slow muscle of lobster reported by Wray (1979). Wray (1979) has discussed the symmetry of the structure of the thick filaments in lobster muscles. Similarly we examined the symmetry of the thick filament structure in the crab muscle taking into account of the 14.5nm meridional, 25.4nm and 33.7nm

off-meridional layer-line reflections due to the thick filaments in the relaxed pattern. The R coordinates of the peaks of these off-meridional reflections were the same, $0.04nm^{-1}$. When these values are conformed to the n-ℓ diagram described by Wray (1979), the first non-zero order of the Bessel function becomes to contribute at $R \simeq 0.23nm^{-1}$ on the equator, far away from the present region of observed reflections. Therefore, the projection of the structure of the thick filaments along the fibre axis should have cylindrical symmetry when derived at the present resolution. Moreover, in the crab muscle, the arrangement of the thin filaments around the thick filament has centre of symmetry. Thus, the above-mentioned assumption for phases seems to be actually valid at the present limited resolution.

Recently, Yagi & Matsubara (1977) studied the cross-sectional structures of the leg muscle of another species of crab (*Plagusia dentipes*) and the abdominal muscle of crayfish. In contrast to our case, they obtained the diffraction patterns with sharp reflections only from the living relaxed muscles and detailed analysis have been made on these muscles in the relaxed state. The thin filament arrangement in the crab muscle used by them was the same as in the muscle used by us and that in the crayfish muscle was the same as in the insect flight muscle (e.g., Reedy, 1968). They observed similar non-staining

appearance in the thick filaments on the electron micrographs of these sectioned muscles. They constructed a cylindrical model with appropriate radii for both filaments which simulated the best-fit to their observed equatorial intensities. The cylindrical model with the hollow thick filaments explained observed features of "strong outer reflections" around the 4,0 and 3,2 reflections in the crab muscle and around 3,1 reflection in the crayfish muscle. Therefore, they concluded that the thick filament has a hollow core in both muscles. On the other hand, we made the Fourier syntheses in the rigor muscle of crab for all combinations of phases of observed reflections and chose possible maps based on the observation by electron microscope that the thin filaments are arranged in the lattice as the model of Fig.I-7(a). As shown in Fig.I-4, we obtained two maps (Figs.I-4(a) and (b)) which show a low electron density core in the thick filament and the other two maps (Figs.I-4(c) and (d)) which show no such a core. We also made Fourier syntheses using the data of the relaxed muscles of crab and crayfish by Yagi & Matsubara (1977). The two kinds of maps similar to Fig.I-4 were resulted for each muscle. This fact suggests that the appearance of "strong outer reflections" in the equatorial pattern is not necessarily an obvious feature of the thick filament with a hollow core. Similar suggestion has also made in insect flight muscle by Holmes, Tregear &

Barrington Leigh (1979). We have determined finally the two Fourier maps of Figs.I-4(a) and (b) which show a low electron density core in the centre of the thick filament based on the observation of electron micrographs from negatively stained isolated thick filament.

Yagi & Matsubara (1977) determined the structural parameters in the living relaxed muscle of crab from their best-fit model as r_A=3.1nm, r_M=9.5nm, r_{MC}=5.7nm. These may be compared with our results in the rigor muscle: r_A=6.2nm, r_M=9.8nm, r_{MC}=3.0nm. It also seems meaningful to compare the structures of both muscles in the Fourier maps. Yagi & Matsubara (1977) constructed a Fourier synthesis at the same resolution of 7nm for the relaxed muscle using phases derived from their best-fit model (Fig.I-8). The phases were the same as ours (Figs.I-4(a) and (b)), except for that of the 3,0 reflection in (b). Fig.I-9 shows the comparison of the electron density distributions along the plane through the centres of the thick and the thin filaments in the Fourier maps. The solid line curve denotes the electron density distribution of the rigor muscle derived from Fig.I-4(a) and the dashed line curve does that of the relaxed muscle calculated using the data of Yagi & Matsubara (1977). These two curves are scaled so as to make the maximum values of the electron density of the thick filaments coincide. The shift of the the electron density peaks of the thin

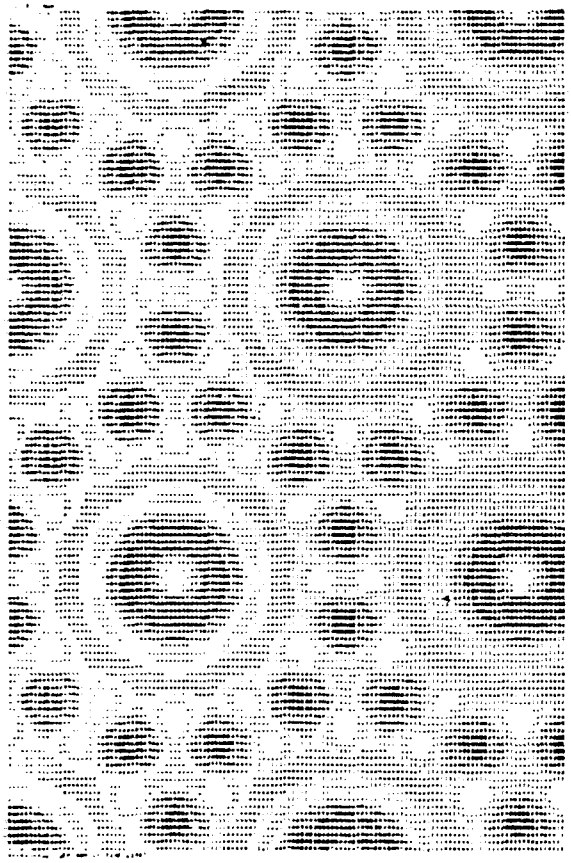

Fig.I-8. Two-dimensional Fourier map of the living relaxed muscle of crab (*Plagusia dentipes*) derived by Yagi & Matsubara (1977).

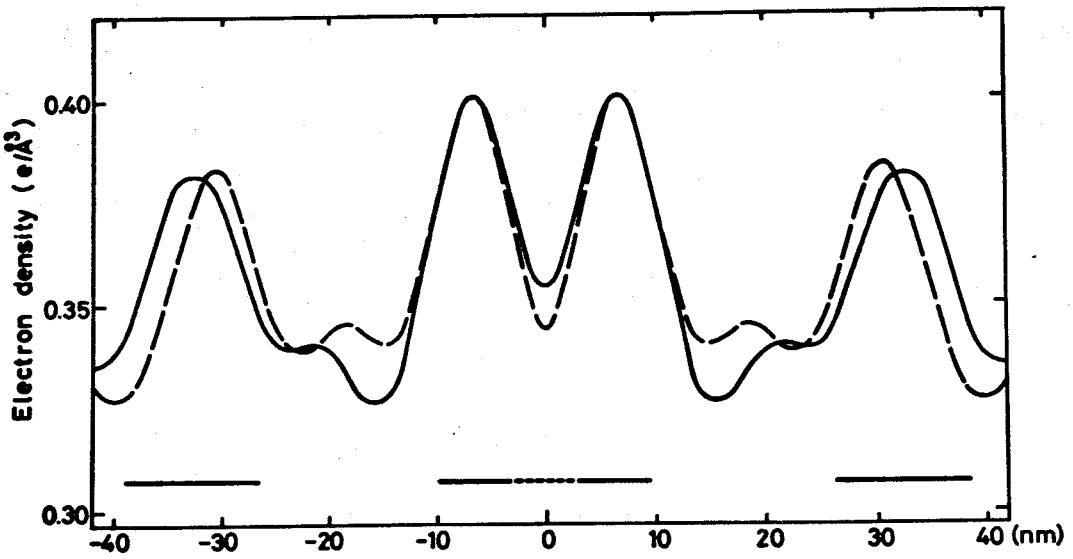

Fig.I-9. Comparison of the electron density distributions along the plane through the centres of the thick and thin filaments. Solid line curve, the rigor muscle; dashed line curve, the relaxed muscle (Yagi & Matsubara, 1977). Electron density is expressed in an absolute scale. Lattice constants are 63nm for the rigor muscle and 59nm for the relaxed muscle. Central bar denotes the thick filament in which dashed part indicates the core, and two bars on either side the thin filaments. The lengths of bars show the size of the filaments determined by our step function model.

filaments is due to the difference of the lattice constants of these muscles. As shown in Fig.I-9, the electron density distribution in the region within 10nm in radius from the centre of the thick filament is almost the same for both muscles. The differences in the electron density between the relaxed and the rigor muscles are present in the thin filaments and in the region between 10nm to 20nm in radius from the centre of the thick filament. Larger spread of the electron density of the thin filaments in the solid line curve could be caused by myosin heads attaching to the thin filaments in the rigor state. The relatively high electron density region around 10nm to 20nm in radius from the centre of the thick filament in the dashed line curve seems to correspond to the position of myosin projections in the relaxed state. Thus the region within 10nm in radius from the centre of the thick filaments corresponds to that of the thick filament backbone, but not including myosin projections. The value 9.5nm of the radius of the thick filament determined by Yagi & Matsubara (1977) in the relaxed muscle seems to correspond to that of the backbone, though they have included the possible contribution from the projections in their model. It should be noted that the thick filament cores of these muscles have quite similar electron density profiles. As mentioned previously, in their step function model the diameter was much larger and that of the thin filament

was much smaller than in our model. However, such large differences between them were not observed in the Fourier maps.

According to the biochemical studies by Maéda et al. (1979) and Wakabayashi et al. (unpublished results), the thick filaments in the crab leg muscles contain paramyosin. It has been suggested for molluscan muscles and for insect muscles that paramyosin is present in the backbone of the thick filament and forms a core around which myosin molecules pack (Lowy & Hanson, 1962; Lowy, Millman & Hanson, 1963; Hardwicke & Hanson, 1971; Szent-Györgyi et al., 1971; Auber & Couteax, 1963). Although we could not offer the definite structural clue to the packing of paramyosin in the thick filament, paramyosin might form a hollow core of 6nm in inner diameter around which the myosin molecules pack. Otherwise it might be present in the core of the thick filament in the bare zone and the beginning of the I region in which the non-staining core is not often seen in the electron micrographs (Millman & Bennett, 1976). Recently, Bullard et al. (1977) reported that antibody to paramyosin bound strongly to the thick filaments in the H-zone in the insect flight muscle.

Appendix

We assumed that the mean electron density of proteins constructing the myofilaments determined by changing the electron density of the solvent is equal to the maximum electron density of the thick filament in the Fourier map. The validity of this assumption is discussed in more detail.

We denoted several variables as follows. ρ_p; the mean electron density of protein molecule, ρ_s; the electron density of solvent, $\mathbf{r}$; the position vector in the real space, x, y, z; the Cartesian coordinate, z being parallel to the fibre axis, $\mathbf{R}$; the position vector in the reciprocal space, X, Y, Z; the Cartesian coordinate, $\rho(\mathbf{r})$; the electron density distribution, $s(\mathbf{r})$; the shape function of the filament, having the value 1 within the volume of the filament and 0 outside, $I(\mathbf{R})$; the intensity distribution. When the mean electron density of individual constituent molecules is not so much different, $\rho(\mathbf{r})$ can be represented as

$$\rho(\mathbf{r}) = \rho_p s(\mathbf{r}) + \rho_s\{1 - s(\mathbf{r})\}. \qquad \text{(I-1)}$$

$\bar{\rho}(x,y)$ is defined by

$$\bar{\rho}(x,y) = \frac{1}{c}\int_0^c \rho(\mathbf{r})dz, \qquad \text{(I-2)}$$

where c is a period of the structure of the filament along the fibre axis. From Eqs.(I-1) and (I-2), we obtain

$$\bar{\rho}(x,y) = (\rho_p - \rho_s)\bar{s}(x,y) + \rho_s \ , \qquad \text{(I-3)}$$

where

$$\bar{s}(x,y) = \frac{1}{c}\int_0^c s(\mathbf{r})dz \leqq 1. \qquad \text{(I-4)}$$

$\bar{\rho}(x,y)$ corresponds to the electron density distribution derived by Fourier transformation of the equatorial intensity data. It is evident from Eq.(I-3) that $\bar{\rho}(x,y)$ is determined by $\bar{s}(x,y)$, and $\bar{s}(x,y)$ would depend on the packing manner of the constituent molecules in each filament along the fibre axis. If $\bar{s}(x,y)=1$ at a certain position (x_1,y_1), $\bar{\rho}(x_1,y_1)=\rho_p$ from Eq.(I-3). This means that the molecules are most closely packed in the filaments along the line parallel to the z-axis at the position (x_1,y_1). We also define $\Delta\rho(\mathbf{r})$ as follows,

$$\Delta\rho(\mathbf{r}) = \rho(\mathbf{r}) - \bar{\rho}(x,y). \qquad \text{(I-5)}$$

From Eqs.(I-1) and (I-3), we obtain

$$\Delta\rho(\mathbf{r}) = (\rho_p - \rho_s)\{s(\mathbf{r}) - \bar{s}(x,y)\}. \qquad \text{(I-6)}$$

The Fourier transform of $\Delta\rho(\mathbf{r})$ is zero on the equator and contributes only on the layer lines except on the equator (cf. Chapter II-4; Namba et al., 1979). In the scattering theory, it is known that a following relation holds (e.g., see Vainshtein, 1963),

$$\int I(\mathbb{R})\,dv_{\mathbb{R}} = \int \rho^2(\mathbb{r})\,dv_{\mathbb{r}} , \qquad \text{(I-7)}$$

where $dv_{\mathbb{R}}$ and $dv_{\mathbb{r}}$ denote the volume elements in the reciprocal and real spaces, respectively. Substituting Eq.(I-5) into Eq.(I-7), we obtain

$$\int I(\mathbb{R})\,dv_{\mathbb{R}} = \int \{\bar{\rho}^2(x,y) + \Delta\rho^2(\mathbb{r}) + 2\bar{\rho}(x,y)\Delta\rho(\mathbb{r})\}dv_{\mathbb{r}} . \qquad \text{(I-8)}$$

In Eq.(I-8), the integral of the third term is zero, and thus we obtain

$$\int I(\mathbb{R})\,dv_{\mathbb{R}} = \int \bar{\rho}^2(x,y)\,dv_{\mathbb{r}} + \int \Delta\rho^2(\mathbb{r})\,dv_{\mathbb{r}} . \qquad \text{(I-9)}$$

$I(\mathbb{R})$ is rewritten by

$$I(\mathbb{R}) = \sum_{\ell} I_{\ell}(X,Y), \qquad \text{(I-10)}$$

where ℓ denotes the layer-line index and $I_{\ell}(X,Y)$ the intensity distribution on the ℓth layer line. Then the terms on the right hand side in Eq.(I-9) are represented respectively by

$$\int \bar{\rho}^2(x,y)\,dv_{\mathbb{r}} = \int I_0(X,Y)\,dX\,dY, \qquad \text{(I-11)}$$

and

$$\int \Delta\rho^2(\mathbb{r})\,dv_{\mathbb{r}} = \sum_{\ell\neq 0} \int I_{\ell}(X,Y)\,dX\,dY. \qquad \text{(I-12)}$$

According to Eqs.(I-5) and (I-6), in Eq.(I-9) if the second term (i.e., Eq.(I-12)) is much smaller than the first term (i.e., Eq.(I-11)), we can regard that $\bar{s}(x,y)$ nearly equal

to 1. As mentioned in the text, in the layer-line diffraction pattern from the rigor muscle, many reflections due to the thin filaments were distinctly observed and those due to the thick filaments were hardly observed except for a few weak reflections (cf. Chapter II; Namba et al, 1979). This fact indicates that $\bar{s}(x,y)$ is nearly equal to 1 for the thick filament backbone and lower than 1 for the thin filaments. This is consistent with the fact that the electron density of the outer part of the thick filament was greater than that of the thin filament in the Fourier maps of Figs.I-4(a) and (b). From Eq.(I-3), when $\bar{s}(x,y) \simeq 1$, $\bar{\rho}(x,y) \simeq \rho_p$ and thus the constituent molecules in the thick filament backbone are most compactly packed. Therefore, it is reasonable to assume that the maximum electron density of the thick filament in the Fourier maps of Figs.I-4(a) and (b) is equal to the mean electron density ($0.4e/\mathring{A}^3$).

CHAPTER II

X-RAY STRUCTURE ANALYSIS OF THE THIN FILAMENT IN THE RIGOR STATE

Summary

X-ray diffraction studies were made on glycerinated leg striated muscles of marine crab, *Portunus trituberculatus*, in the rigor and relaxed states. In the rigor state, many distinct layer lines with the basic period of 76.5nm due to the thin filaments were observed, well separated from several relatively weak layer lines with the basic period of 14.5nm caused by the thick filaments. In the relaxed state, most of the layer lines due to the thin filaments became very weak.

No lattice sampling effect was observed on any layer lines, except on the equator. Layer-line spacings proved that the F-actin helix in the thin filament has 28 subunits in 13 turns.

Structure analysis of the thin filament in the rigor state was made by using thirteen layer-line reflections measured with reasonably good accuracy. The analysis was largely helped by a difference Patterson function $\Delta Q(\mathbf{r})$ defined by $\Delta Q(\mathbf{r}) = Q(\mathbf{r}) - (1/c)\int_0^c Q(\mathbf{r})dz$, where $Q(\mathbf{r})$ is the Patterson function, $\mathbf{r}$ the position vector, z the coordinate parallel to the fibre axis and c the period of the filament. Results showed that, in the rigor state, the myosin heads attach periodically along the thin filament: they are bound to 3, 3', 4, 4' and 10, 10', 11, 11' actin monomers when the actin monomers are numbered as $1 \sim 14$ along one strand of the long-pitch helix and $1' \sim 14'$ along

the other, 1' being neighboured by 1 and 2. Troponin molecules sit on the filament laying their centres of gravity at roughly the same z coordinates as 1, 1' and 8, 8' actin monomers, or as 5', 6 and 12', 13 as another possibility.

Several theorems are given on $\Delta Q(r,z)$, which would be generally useful in analysis of fibre structures.

II-1. Introduction

The contraction of striated muscles results from the sliding of the thin filaments along the thick filaments, which is caused by the alternate formation and breaking of cross-links between the actin and myosin molecules (Huxley & Niedergerke, 1954; Huxley & Hanson, 1954; Huxley, 1957, 1971; Huxley, 1960, 1969, 1971). Dynamical X-ray diffraction studies will be essential for studies of the dynamical behaviour of the crossbridge. Nevertheless, the knowledge of the structure of muscle in the rigor state will be of some help to understand the mechanism of the crossbridge formation. This Chapter presents our results on the structure of the thin filament of crab striated muscle in the rigor state.

Small-angle X-ray diffraction studies have been extensively made on the relaxed and rigor states of vertebrate striated muscles (e.g., Huxley & Brown, 1967), insect flight muscles (Miller & Tregear, 1972; Goody et al., 1975; Barrington Leigh et al., 1977; Tregear et al., 1979; Holmes et al., 1979), limulus, lobster and crayfish striated muscles (Wray, Vibert & Cohen, 1974, 1975, 1978; Wray, 1979), scallop striated muscle (Millman & Bennett, 1976) and crab striated muscles (Maéda, 1979; Maéda et al., 1979; Namba, Wakabayashi & Mitsui, 1979). The diffraction patterns from these muscles have several common features. In the relaxed muscles, the layer lines due to the thick

filaments are distinct, suggesting a regular arrangement of the projected myosin heads around the thick filament. In the rigor muscles, the layer lines due to the thin filaments become enhanced and the layer lines due to the thick filaments are weakened, indicating that the head parts of myosin molecules bind to the thin filaments keeping the basic structure of F-actin filament unchanged (Huxley & Brown, 1967).

Reedy (1967, 1968) pointed out that the myosin heads attach to the thin filaments at regular intervals of 38.8nm along the filament axis in the rigor insect flight muscle on the basis of his observation by electron microscopy. For about ten years since his indication, however, regular attachment of myosin heads had not been taken into account in interpretation of X-ray diffraction pattern of any muscles. It was because of prejudice that the rigor structure is the irregular one caused by the vernier relation of the thick and the thin filament of which periodicities are quite different. Recently several authors have supported his idea based upon X-ray diffraction in the insect flight muscle (Barrington Leith et al., 1977; Holmes et al., 1979), and in other arthropod muscles (Wray et al., 1978; Maéda, 1979; Namba et al., 1979).

X-ray diffraction patterns by insect or crustacean muscles in the rigor state are very distinct, and lead us to temptation to search a way to reach structural models

of these muscles with least ad hoc assumptions. Such an approach has been made, for instance, by Barrington Leigh et al. (1977) and Holmes et al. (1979) with the idea of longitudinal modulation function. In this Chapter, I propose another way of such an approach based upon a modified Patterson function and to present a structural model of the thin filament of crab muscle in the rigor state.

II-2. Materials and Methods

(a) Specimens

Same muscle as described in Chapter I-2 was used. The muscle fibre was used after glycerination. X-ray specimens were almost a single fibre in this experiment. The thickness of the single fibre was about 300μm. The muscle fibre was mounted in specimen holder which was thermoelectrically cooled to 4°C with a Coolnics (Komatsu Yamato Co., Tokyo). Chilled rigor solution or relaxing solution was circulated in the cell with a peristaltic pump during X-ray exposure, so that we could obtain X-ray diffraction patterns of the same specimen either in the rigor state or in the relaxed state. Two kinds of solutions have been described in Chaper I-2. X-ray experiments were done at the rest length of the muscle. Its sarcomere length was determined as about 5.5μm by light diffraction patterns using a He-Ne gas laser (NEC, GLG2026, Tokyo).

Observation with a phase contrast microscope showed that the A-band occupied 70 ∿ 80% of the sarcomere length.

(b) X-ray diffraction

Two X-ray sources were used: Rigaku Denki rotating anode microfocus generators RU3HM and RU100 with copper targets, operated at 55kV with a tube current of 6mA (RU3HM) and 40kV with that of 30mA (RU100). The focal size viewed at angle of 6° was approximately 100 × 100μm^2. The mirror-monochromator camera described in Chapter I was used to record diffraction patterns. The specimen was located at the distances ranging 10 ∿ 32cm from the film depending upon required resolution. The incident X-ray beam was perpendicular to the muscle fibre. In order to get the good resolution in the direction of fibre axis and to use the X-ray beam effectively, the fibre was set parallel to the focusing direction of monochromator. Sakura industrial N and Ilford industrial G films were used. The exposure time was around 50 ∿ 70hr. Diffraction spacings were calibrated by the powder pattern of sodium myristate (cf. International Table for X-ray Crystallography ed. Kasper and Lonsdale, Vol. III, p.331 (1968)).

(c) Intensity data

The optical density of the film was measured on a Nalumi C-type densitometer. Slit size was 20 × 50μm^2.

Scanning was made perpendicularly to the layer lines in the range of $0.25nm^{-1}$ at an interval of $0.01nm^{-1}$, in terms of the reciprocal radial coordinate R (cf. the cylindrical coordinates defined later). The optical density was converted to the scattered X-ray intensity with the help of a standard scale. Background intensity was then subtracted. Subsidiary visual estimation of layer-line intensity was made by comparison with an intensity scale (Franklin & Gosling, 1953), especially at the place where background was high. The area under the peak was adopted as an integrated intensity. The Lorentz correction was not applied to the intensities on the layer lines since the calculations were made upon cylindrically averaged intensities as described later.

(d) Calculations

Calculations were carried out on the ACOS 77-NEAC SYSTEM 700 Computer at the Computer Centre of Osaka University.

II-3. Experimantal Results

Fig.II-1 shows low-angle X-ray diffraction patterns of the glycerinated crab muscles in the rigor state (a) and the relaxed state (b). Two sets of layer-line reflections are present in these diffraction patterns,

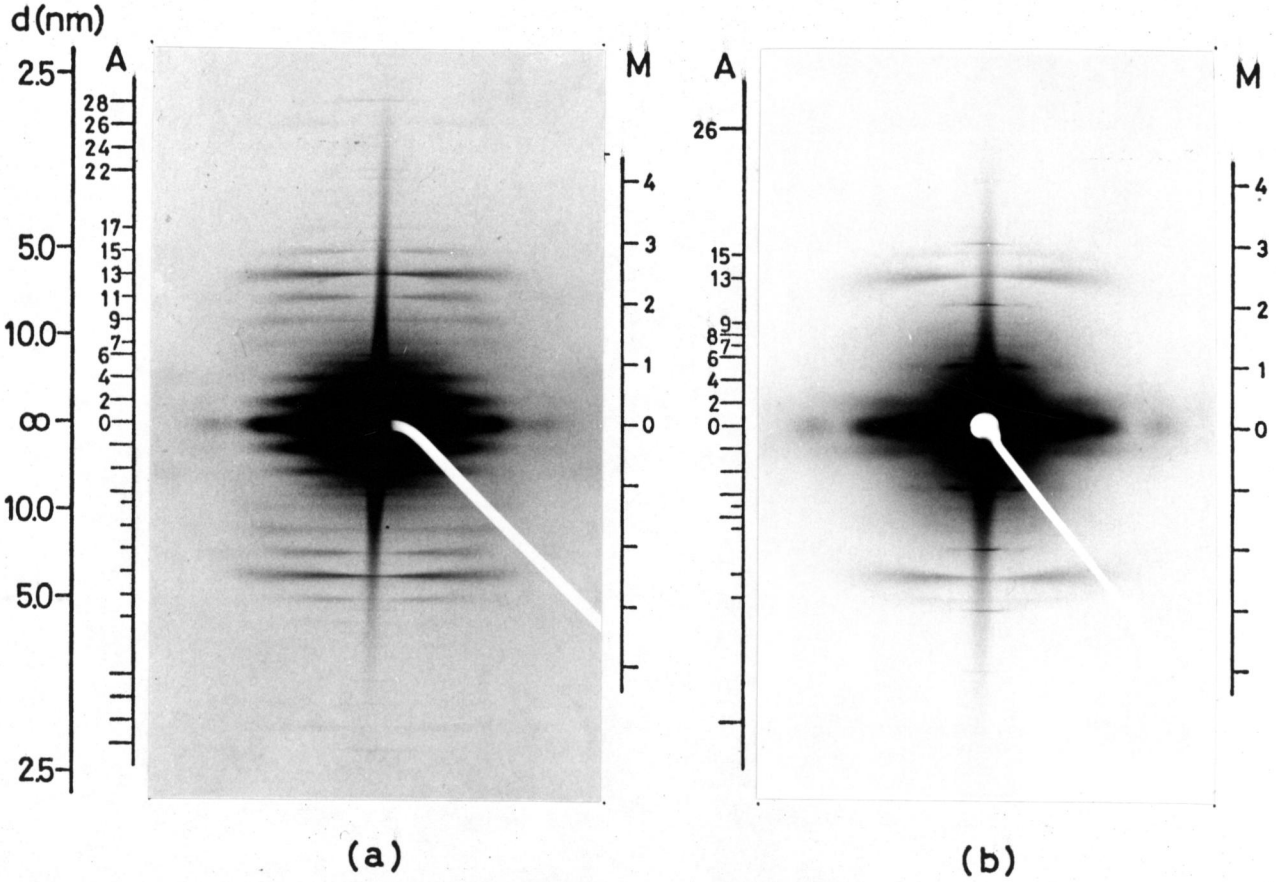

Fig.II-1. Small-angle X-ray diffraction photographs of crab leg striated muscle. (a) the rigor state. (b) the relaxed state. Fibre axis, vertical; specimen-to-film distance, 32cm; exposure time, 70hr. A, layer lines of the thin filament; M, Those of the thick filament; numbers of the A and M scales, order of layer-line reflection; d, spacing. The strong nearly vertical line was caused by parasitic scatterings.

corresponding to the basic periods of 14.5nm and 76.5nm. The reflections with the periods of 14.5nm and 76.5nm should be attributed to the thick and thin filaments, respectively. Calculation of layer-line spacings with these periods proved that the reflections of the two sets are well separated without serious overlap in the low-angle region covered by Figs.II-1(a) and (b), due to different periodicities of the thick and thin filaments. These periods are common in the rigor and relaxed muscles, suggesting that the helical structure of F-actin is not deformed largely in both the rigor and relaxed states.

Fig.II-1(a) shows many strong layer-line reflections due to the thin filaments. The 13th layer line has the spacing of 5.89nm, which is expected to be the pitch of the genetic helix of F-actin. The meridional 28th layer-line reflection has the spacing of 2.73nm, which corresponds to the axial repeat of the actin monomers in the F-actin filament. The ratio $5.89/2.73 \simeq 28/13$ indicates that the F-actin in the thin filament can be looked upon as a helix with 28 subunits in 13 turns. The selection rule for this left-handed helix is given by $\ell = -13n + 28m$, where ℓ denotes the layer-line index and n is the order of Bessel function. In Fig.II-1(a), four weak meridional reflections could be assigned as the 1st $\sim$ 4th order reflections with the basic period of 14.5nm. They are due to the thick filaments. In the relaxed state

(Fig.II-1(b)), their intensities increase and subsidiary off-meridional maxima become visible on the same layer lines. Also higher-order reflections appear in the relaxed state although they can hardly be seen in Fig.II-1(b). Two additional off-meridional layer lines of which spacings are 25.4nm and 33.7nm can be seen in relaxed state. The former is not distinguishable from the 3rd order layer line of the thin filament. These layer lines can be, however, refer to the helical arrangement of the projection of the thick filament, because they disappear in the rigor state.

Figs.II-2(a) and (b) show the moderate-angle diffraction patterns for the rigor and relaxed muscles, respectively. Distinct layer line reflections in the wide-angle range which is not covered by Figs.II-1(a) and (b) were assigned as the reflections for $n = 0$ or ± 1 in the selection rule of $\ell = -13n + 28m$. There is no appreciable change in sharpness of these reflections in Figs.II-2(a) and (b). There are, however, several changes in their intensities. The 28th layer line can be clearly seen in the rigor state (Figs.II-1(a) and II-2(a)) but disappears in the relaxed state (Figs.II-1(b) and II-2(b)). Intensity on the layer line of $\ell = 41$ ($n = -1$, $m = 1$) decreases and that of $\ell = 43$ ($n = 1$, $m = 2$) increases from the rigor state to the relaxed state, making their relative intensities reversed.

One striking feature of Fig.II-1 is that the lattice

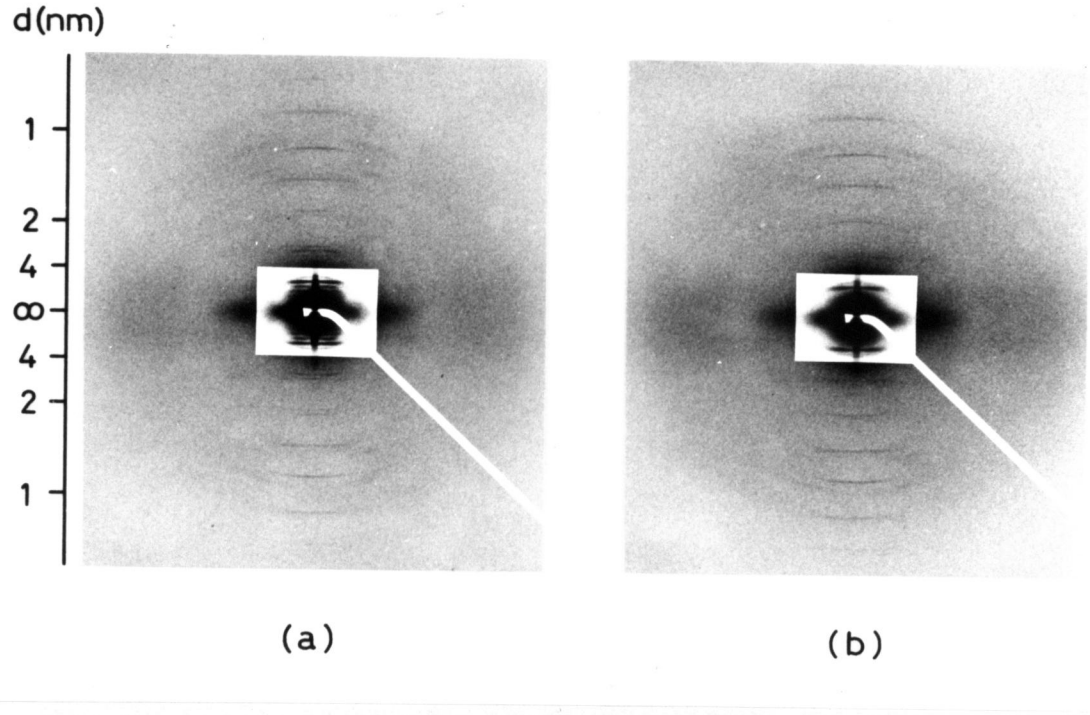

Fig.II-2. Moderate-angle diffraction photographs of crab leg striated muscle. (a) the rigor state. (b) the relaxed state. Fibre axis, vertical; specimen-to-film distance, 10cm; exposure time, 70hr; d, spacing.

sampling effect is absent on any layer lines except on the equator, unlike the frog skeletal muscle (Huxley & Brown, 1967), the insect flight muscle (Miller & Tregear, 1972; Barrington Leigh et al., 1977) and other crustacean muscles (Wray et al., 1975, 1978).

Diffraction photographs were taken with the same specimen in the rigor and relaxing solutions for the same exposure time. Intensities of the layer-line reflections due to the thin filaments were measured by the densitometer with the help of visual estimation in the low-angle range covered by Figs.II-1(a) and (b). Results are given in Fig.II-3. In the present study, our main concern is the structure of the thin filament, and intensities were not measured on the layer lines due to the thick filaments. Fig.II-3 gives intensities on the layer lines of ℓ = 2, 4, 6, 7, 9, 11, 13, 15, 17, 22, 24, 26, 28 in the rigor state (a) and those on the layer lines of ℓ = 2, 4, 6, 7, 8, 9, 13, 15 in the relaxed state (b). In the relaxed state, it was difficult to measure intensities of the layer-line reflections with ℓ = 4, 6, 7, 8, 9 with the densitometer due to their weakness and the relatively high background around them. Therefore, their intensities were estimated visually by comparison with a standard scale as described in the preceding section.

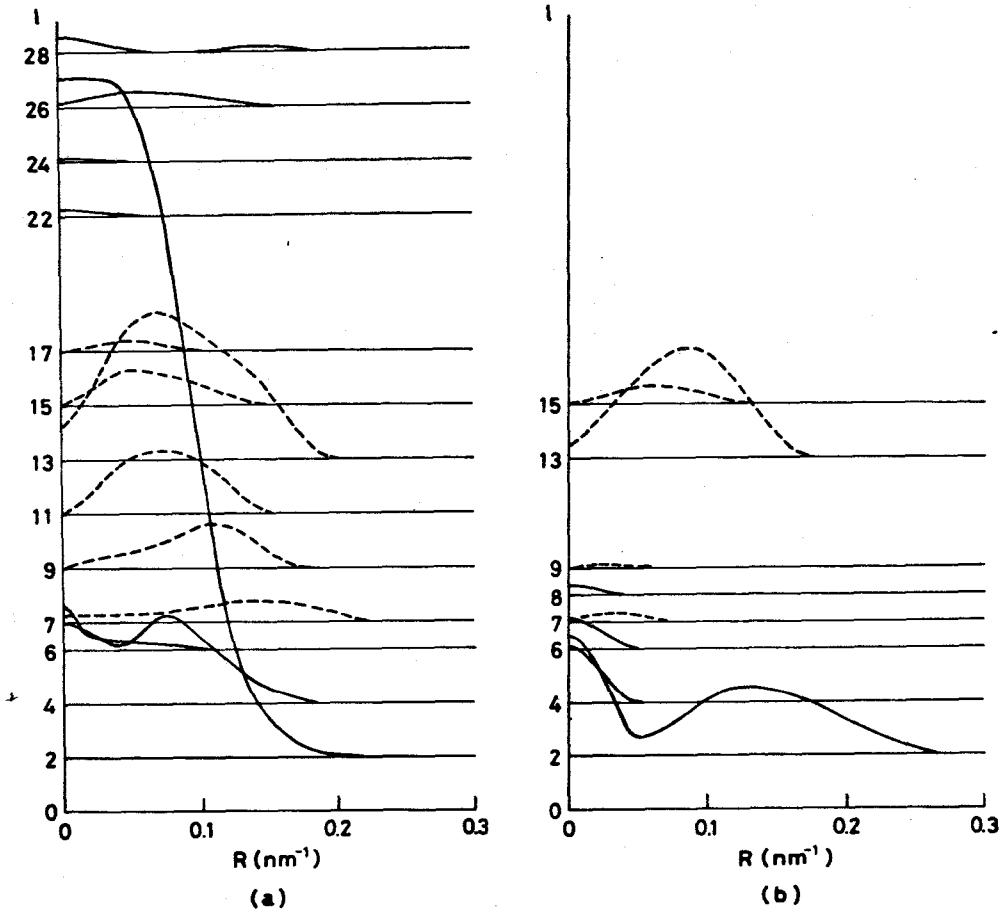

Fig.II-3. Observed $I_\ell(R)$ due to the thin filaments. (a) the rigor state. (b) the relaxed state. Full line, $I_\ell(R)$ for ℓ = even; dashed line, ℓ = odd. Origin of each $I_\ell(R)$ sits on the corresponding layer line.

II-4. Structure Analysis

The muscle gave well defined Bragg peaks on the equator, indicating that the projection of the muscle structure along the fibre axis forms a regular hexagonal lattice (cf. Chapter I; Wakabayashi & Namba, 1978). As mentioned in the preceding section, however, no distinct lattice sampling effect was observed on any layer lines except on the equator, indicating that the myofibrils do not form a three-dimensional lattice. Therefore, we treated the observed diffraction intensities as the cylindrically averaged intensities diffracted by a single filament.

(a) Basic properties of a difference cylindrically symmetrical Patterson function

McGillavry & Bruins (1948) pointed out that the cylindrically symmetrical Patterson function would be useful in X-ray structure analysis of fibre materials. Franklin & Gosling (1953) used this function in studies of DNA, determined the unit cell parameters and discussed a possible shape of the fundamental structural unit. Since then several authors used this function in analysis of biological structures as cited in Vainshtein's textbook (1966). We have tried to analyse the crab muscle structure by this method, and found that a difference cylindrically symmetrical Patterson function $\Delta Q(r,z)$ given later by

Eq.(II-14) is very useful in extracting information on muscle structure from the X-ray data. Since our analysis largely depends upon this function, the basic properties on $\Delta Q(r,z)$ are presented here before going into discussion on the crab muscle structures.

Suppose a fibre specimen which has a periodic structure along the fibre axis with the period c. When an X-ray beam is incident perpendicularly to the fibre axis, the layer-line reflections are caused. Below we shall use the following notations: $\mathbf{r}$, the position vector in real space; x, y, z, the orthogonal Cartesian coordinates; r, ϕ, z, the cylindrical coordinates; $\mathbf{R}$, the position vector in reciprocal space; X, Y, Z, the orthogonal Cartesian coordinates; R, Φ, Z, the cylindrical coordinates; $\rho(\mathbf{r})$, the electron density distribution; $Q(\mathbf{r})$, the autocorrelation function of $\rho(\mathbf{r})$; $I(\mathbf{R})$, the intensity distribution of scattered X-rays. Definition of $Q(\mathbf{r})$ is

$$Q(\mathbf{r}) = \int \rho(\mathbf{r}')\rho(\mathbf{r}'+\mathbf{r})dv_{\mathbf{r}'} , \qquad \text{(II-1)}$$

where $dv_{\mathbf{r}'}$ is the volume element. $Q(\mathbf{r})$ is called the Patterson function in crystal structure analysis. $Q(\mathbf{r})$ can be calculated by

$$Q(\mathbf{r}) = \int I(\mathbf{R})\exp(2\pi i\mathbf{R}\mathbf{r})dv_{\mathbf{R}} . \qquad \text{(II-2)}$$

In our case $I(\mathbf{R})$ is non-zero only near the planes at $z = \ell/c$ where ℓ are integers. We define $I_\ell(R,\Phi)$ by

$$I_\ell(R,\Phi) = \int_{\ell/c-\varepsilon}^{\ell/c+\varepsilon} I(\mathbf{R})dz, \qquad \text{(II-3)}$$

where $\varepsilon<1/(2c)$. We shall use the following quantities.

$$\bar{\rho}(x,y) = \frac{1}{c}\int_0^c \rho(\mathbf{r})dz, \qquad \text{(II-4)}$$

$$\Delta\rho(\mathbf{r}) = \rho(\mathbf{r}) - \bar{\rho}(x,y), \qquad \text{(II-5)}$$

$$\bar{Q}(x,y) = \frac{1}{c}\int_0^c Q(\mathbf{r})dz, \qquad \text{(II-6)}$$

$$\Delta Q(\mathbf{r}) = Q(\mathbf{r}) - \bar{Q}(x,y). \qquad \text{(II-7)}$$

Eq.(II-7) defines a difference patterson function. Concerning these quantities we have the following theorems.

[Theorem 1]

$$\Delta Q(\mathbf{r}) = \int \Delta\rho(\mathbf{r}')\Delta\rho(\mathbf{r}'+\mathbf{r})dv_{\mathbf{r}'}. \qquad \text{(II-8)}$$

This means that $\Delta Q(\mathbf{r})$ is the autocorrelation function of $\Delta\rho(\mathbf{r})$. This theorem can be proved with Eqs.(II-1), (II-5) and (II-7).

[Theorem 2]

$\Delta Q(\mathbf{r})$ can be calculated without information of $I_0(R,\Phi)$:

$$\Delta Q(\mathbf{r}) = \sum_{\ell\neq 0=-\infty}^{\infty} \{\int_{-\infty}^{\infty} I_\ell(X,Y)\exp(2\pi i(xX+yY))dXdY\}\exp(2\pi i\ell z/c). \qquad \text{(II-9)}$$

This theorem can be proved with Eqs.(II-2),(II-3) and (II-7).

[Theorem 3]

The ϕ-average of $Q(\mathbf{r})$ can be calculated by using the Φ-average of $I_\ell(R,\Phi)$:

$$Q(r,z) = \sum_{\ell=-\infty}^{\infty} \{\int_0^{\infty} I_\ell(R) J_0(2\pi Rr) 2\pi R dR\} \exp(2\pi i \ell z/c), \quad \text{(II-10)}$$

where

$$Q(r,z) = \int_0^{2\pi} Q(r,\phi,z) d\phi, \quad \text{(II-11)}$$

$$I_\ell(R) = \int_0^{2\pi} I_\ell(R,\Phi) d\Phi, \quad \text{(II-12)}$$

and $J_0(2\pi Rr)$ is the zeroth order of Bessel function with the argument $2\pi Rr$. This theorem is due to McGillavry and Bruins (1948). $Q(r,z)$ is called the cylindrically symmetrical Patterson function. Eq.(II-10) can be rewritten as

$$Q(r,z) = \int_0^{\infty} I_0(R) J_0(2\pi Rr) 2\pi R dR + 2\sum_{\ell=1}^{\infty} \{\int_0^{\infty} I_\ell(R) J_0(2\pi Rr) \times 2\pi R dR\} \cos(2\pi \ell z/c). \quad \text{(II-13)}$$

[Theorem 4]

$$\Delta Q(r,z) = 2\sum_{\ell=1}^{\infty} \{\int_0^{\infty} I_\ell(R) J_0(2\pi Rr) 2\pi R dR\} \cos(2\pi \ell z/c), \quad \text{(II-14)}$$

where

$$\Delta Q(r,z) = \int_0^{2\pi} \Delta Q(r,\phi,z) d\phi. \quad \text{(II-15)}$$

This theorem can be proved by use of Eqs.(II-9) and (II-13). We shall call $\Delta Q(r,z)$ the difference cylindrically

symmetrical Patterson function. As mentioned in Chapter I, our muscle gave well defined Bragg peaks on the equator, indicating that the projection of muscle structure along the fibre axis forms a regular hexagonal lattice and thus X-rays scattered by the thin and thick filaments interfere with each other (cf. Chapter I; Wakabayashi & Namba, 1978). By definition, as in the cases of other $I_\ell(R)$, $I_0(R)$ is the X-ray intensity scattered by a single thin filament (and thus a non-Bragg, continuous function). Therefore, $I_0(R)$ is not available experimentally in our case. The theorem 4 means that even in such a case one can calculate $\Delta Q(r,z)$ as $I_\ell(R)$ of $\ell \neq 0$ are available experimentally.

By definition of Eq.(II-5), $\Delta\rho(\mathbf{r})$ stands for deviation of $\rho(\mathbf{r})$ from the z-average of $\rho(\mathbf{r})$, i.e., $\bar{\rho}(x,y)$. Therefore, $\Delta\rho(\mathbf{r})$ may have a large value where a heavy molecule sits. According to Eq.(II-8), $\Delta Q(\mathbf{r})$ is the autocorrelation function of $\Delta\rho(\mathbf{r})$, and thus there may appear a high peak on the contour map of $\Delta Q(r,z)$ corresponding to a vector connecting heavy molecules. Therefore, we have the following theorem.

[Theorem 5]

When there appear distinct peaks on the contour map of $\Delta Q(r,z)$, their positions indicate r and z components of the vectors connecting heavy molecules.

By this theorem we may use $\Delta Q(r,z)$ in a way analogous to

the Patterson function in crystal structure analysis if its contour map exhibits distinct peaks.

In the following discussion we shall use the relation,

$$\int_0^c \Delta Q(r,z)dz = 0, \qquad \text{(II-16)}$$

which is obvious from Eq.(II-7).

Fig. II-4 illustrates how contour maps of $Q(r,z)$ and $\Delta Q(r,z)$ look like for a model structure. Fig.II-4(a) shows a simplified model of F-actin having the period c of 76.5nm, with 28 monomers in it. An actin monomer is represented by a sphere of radius 2.4nm and its centre is set at 2.5nm apart from the fibre axis. The selection rule for the structure is given by $\ell = -13n + 28m$. Figs.II-4(b) and (c) shows contour maps of $Q(r,z)$ and $\Delta Q(r,z)$ for this model. (Procedure of the calculations will be given later.) These functions have centres of symmetry at (0,0) and (0,c/2), and thus their contour maps are given only for $0 \leq z \leq c/2$. The crosses on the maps stand for heads of vectors connecting centres of actin monomers in Fig.II-4(a). Peaks appear more distinctly around the crosses in Fig.II-4(c) than Fig.II-4(b), implying that $\Delta Q(r,z)$ might be more useful in analysis of muscle structures even if $Q(r,z)$ were obtained. Eq.(II-16) implies that the contour map of $\Delta Q(r,z)$ should have both positive and negative areas. In Figs.II-4(b) and (c), white area corresponds to positive region, gray area to

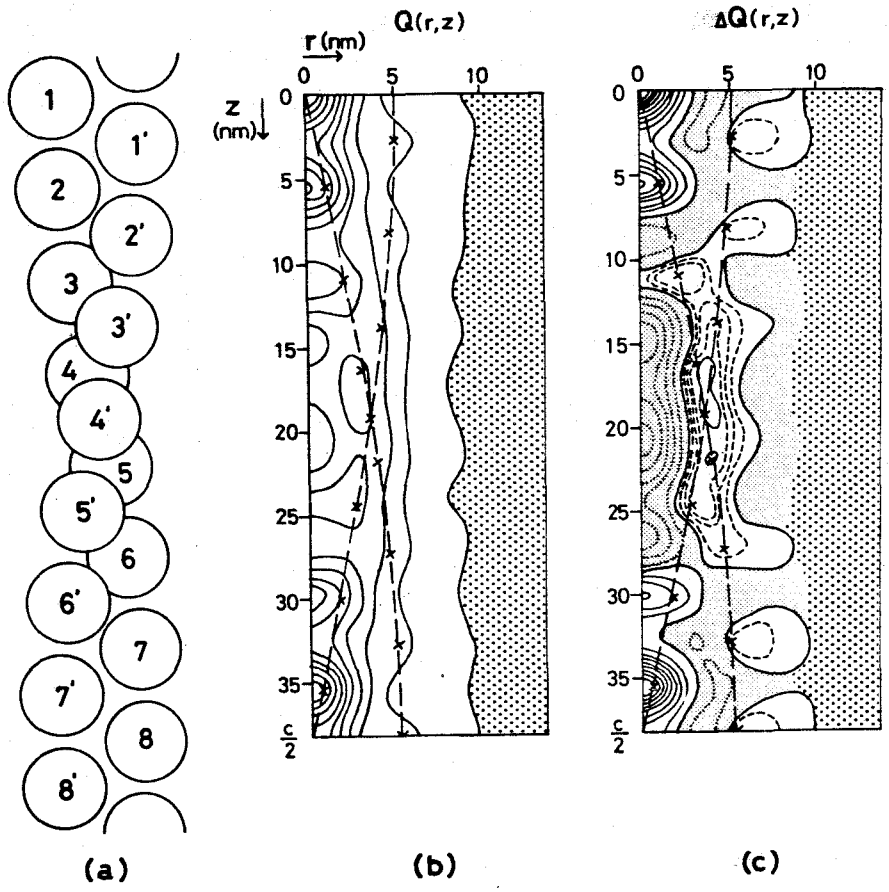

Fig.II-4. Examples of contour maps of $Q(r,z)$ and $\Delta Q(r,z)$. (a) side view of a simple model of F-actin filament. Numbered sircle stands for an actin monomer. (b) contour map of $Q(r,z)$ calculated for the model in (a). (c) contour map of $\Delta Q(r,z)$ calculated for the model in (a). The peaks at the origins were normalized to 1,000 in (b) and (c). Full and dashed lines, positive contour; dotted line, negative contour. Contour interval is 100 for the full and dotted lines, and 25 for the dashed line. White area, positive region; gray area, negative region; dotted area, zero region defined by $Q(r,z) < 1$ and $|\Delta Q(r,z)| < 1$. In (b) and (c), cross stands for a head of vector connecting centres of actin monomers in (a).

negative region and dotted area to zero level. By Eq.(II-1), averaged r coordinate of the boundary between the white and dotted areas in Fig.II-4(b) gives an approximate diameter of the F-actin filament. By Eq.(II-8), the boundary between the non-zero and zero in Fig.II-4(c) gives the same approximate diameter.

(b) Calculations of $\Delta Q(r,z)$ and $Q(r,z)$ from model structures

Here we mention some fundamental equations which we used in calculating $\Delta Q(r,z)$ or $Q(r,z)$ from structural models.

There may be a way to calculate $\Delta Q(r,z)$ or $Q(r,z)$ directly from a model by Eq.(II-8) or (II-1), but we took an indirect way. That is, we calculated $I_\ell(R)$ for a model and then calculated $\Delta Q(r,z)$ or $Q(r,z)$ by Eq.(II-14) or (II-13). $I_\ell(R)$ was calculated following Klug, Crick & Wyckoff (1958). Equations used were as follows.

$$I_\ell(R) = \sum_n \left| \sum_\alpha F_{n\ell}^{(\alpha)}(R) \right|^2, \qquad \text{(II-17)}$$

$$F_{n\ell}^{(\alpha)}(R) = \sum_j f_j^{(\alpha)} J_n(2\pi R r_j) \exp[i\{-n(\phi_j - \tfrac{\pi}{2}) + 2\pi \ell z_j/c\}]. \qquad \text{(II-18)}$$

The molecules were approximated by a sphere or overlapping spheres as was done by Miller & Tregear (1972). The symbol f_j stands for the form factor of jth sphere having the radius of r_0. As was given, for instance, in the paper by Oster & Riley (1952), f_j is expressed by

$$f_j = 3\sqrt{\frac{\pi}{2}} \frac{J_{3/2}(2\pi S r_0)}{(2\pi S r_0)^{3/2}}, \qquad \text{(II-19)}$$

$$S = \{R^2 + (\ell/c)^2\}^{1/2}. \qquad \text{(II-20)}$$

The spheres representing molecules or fractions of molecules can be classified into three categories depending upon the symmetry of the sites of the relevant molecules. The suffix α in Eq.(II-18) specifies this. This symmetry denoted by $\alpha = 1$ corresponds to that of the F-actin, $\alpha = 2$ to bound myosin heads and troponin and $\alpha = 3$ to tropomyosin. In term of the selection rule, $\alpha = 1$ is for $\ell = -13n + 28m$, $\alpha = 2$ is for $\ell = n + 2m$, and $\alpha = 3$ corresponds to a two-strand continuous helix. We took Bessel functions of the order of $|n| < 15$ into account and calculated $I_\ell(R)$ for $\ell \leqq 28$ and $R \leqq 0.4\text{nm}^{-1}$. The model in Fig.II-4(a) consists solely of F-actin and only $F_{n\ell}^{(1)}(R)$ appeared in Eq.(II-17) in calculating $Q(r,z)$ and $\Delta Q(r,z)$ given in Figs.II-4(b) and(c).

(c) The structure of the thin filament in the rigor state

The function $\Delta Q(r,z)$ were calculated for the thin filaments in the rigor and relaxed states by using the intensities $I_\ell(R)$ given in Fig.II-3. Obtained contour maps are shown in Figs.II-5(a) and (b), respectively. As mentioned in the preceding section, the data in Figs.II-3(a) and (b) were obtained with the same muscle fibres immersed

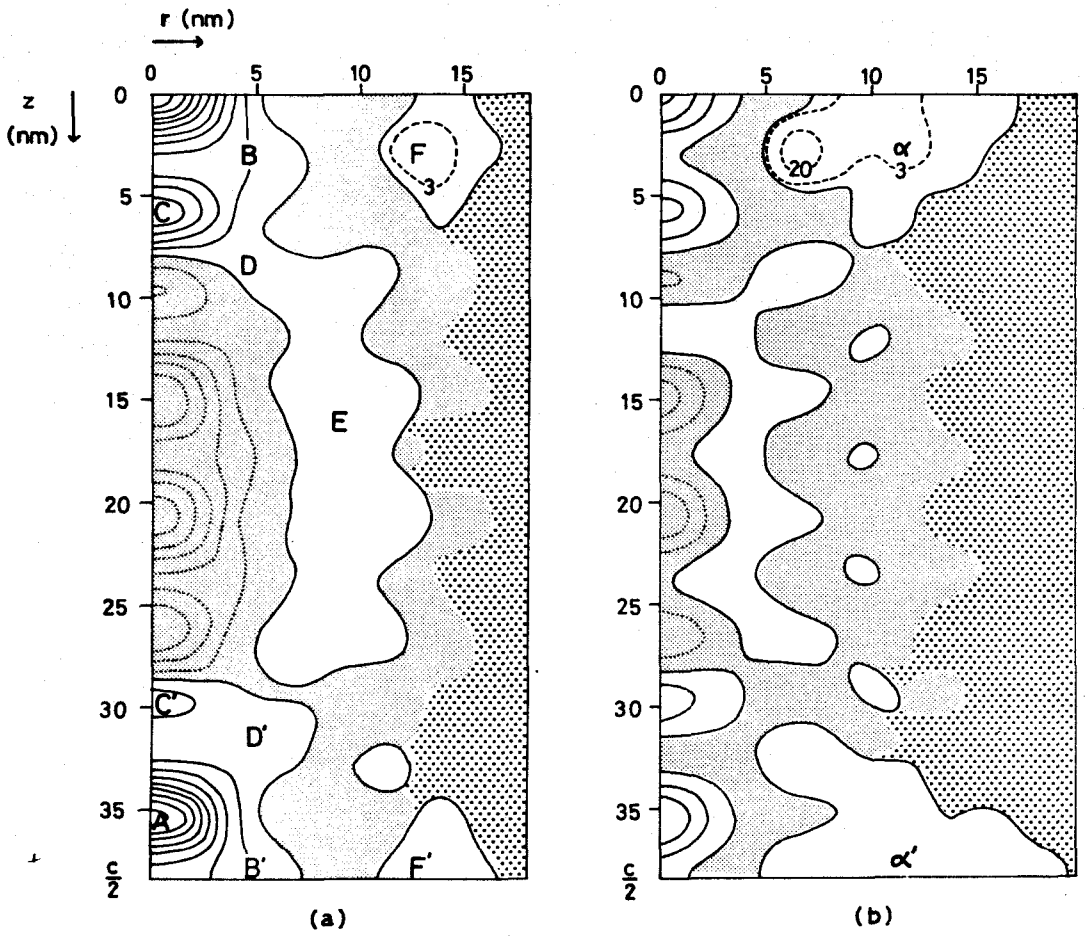

Fig.II-5. Contour maps of $\Delta Q(r,z)$ calculated with observed $I_\ell(R)$ in Fig.II-3. (a) the rigor state. (b) the relaxed state. The scale is common for (a) and (b) (see text). The peak at the origin was normalized to 1,000 in (a). Full line, positive contour; dotted line, negative contour. Contour interval is 100. Contour lines of 3 and 20 are given by dashed lines in the region around F in (a), and in the region around α in (b). Other notations are the same as in Fig.II-4(c). Values at lettered positions are: A, 840; B, 100; B', 100; C, 480; C', 150; D, 20; D', 50; E, 17; F, 6; F', 9 in (a), α, 5; α', 6 in (b).

in the rigor solution or in the relaxing solution, for the same exposure time. A common scale factor was used for these intensity data so as to make quantitative comparison between Figs.II-5(a) and (b) possible. The scale factor was determined to make the peak height at the origin in Fig.II-5(a) 1,000. Pronounced increase of $\Delta Q(r,z)$ takes place in several regions in Fig.II-5(a) compared to Fig.II-5(b): 314 → 1,000 at the origin, 288 → 840 at A, -11 → 100 at B, 235 → 481 at C, 0 → 20 at D, -3 → 17 at E. These changes indicate that the thin filament is decorated heavily by myosin heads in the rigor state. In contrast to these, peak height of the F peak in Fig.II-5(a) is almost the same as that of the α peak in Fig.II-5(b) (6 for F, 5 for α). Here we notice that the extinction rule characteristic to 2_1 screw symmetry is apparent in Fig.II-3: the meridional reflections are present on the layer lines of ℓ = even and absent for ℓ = odd. We shall postulate below that the structure of the thin filament has the 2_1 symmetry.

Among the above-mentioned pronounced increases of $\Delta Q(r,z)$ in Fig.II-5(a), the increase at the A peak is the most distinct and that at the C peak is the second largest except for the origin. The position of the A peak corresponds to the inter-molecular vector of about 35.5nm almost parallel to the z axis. Remembering the theorem 5, such a peak should take place if the 1' and 8 actin monomers

in Fig.II-4(a) would be bound by heavy molecules. (Other combinations, e.g., binding to 1 and 7', etc. lead us to equivalent models.) Then the 2_1 symmetry requires that the 8' and 1 actin monomers should be bound by heavy molecules. The position of the C peak in Fig.II-5(a) corresponds to the vector connecting 1 and 2 actin monomers, or 1', 2; 8, 9; 8',9'. Therefore, Fig.II-5 suggests one possible model that 1, 1', 2, 2', 8, 8', 9, 9' actin monomers are bound by myosin heads in the rigor state. Making this suggestion as a starting point, we tried to interpret all features of $\Delta Q(r,z)$ in Fig.II-5(a) with various trial models. Firstly, it was assumed that the way for a myosin head binds to an actin monomer is the same as assumed by Miller & Tregear (1972) as far as a single binding is concerned. The myosin head corresponds to the subfragment-1 (S1) according to them, and was approximated as a rod about 5.6nm wide and 17nm long. Various models were examined as well as the above-described combination: (1) myosin heads bind to 1, 1', 2, 2', 8, 8', 9, 9' actin monomers; (2) to 1, 1', 8, 8'; (3) to 1, 1', 2, 2', 3, 3', 8, 8', 9, 9', 10, 10'; (4) to more actin monomers. In Miller-Tregear's way of binding, however, the vectors connecting opposite S1 (e.g., the ones attached to the 1 and 1' actin monomers) give a flat peak at very large r coordinate ($10\text{nm} \lesssim r \lesssim 30\text{nm}$) around the z coordinate ($-9\text{nm} \lesssim z \lesssim 9\text{nm}$), where the positive area does not extend in Fig.II-5(a).

Therefore, we reduced the r coordinate of centre of gravity of S1 in the model so that it could give a peak at the F position in Fig.II-5(a). Again we examined various models and got relatively good resemblance in appearance between calculated $\Delta Q(r,z)$ and Fig.II-5(a) for the above-mentioned combination of (1), as expected. Fig.II-6 shows an example of such models, in which the way of S1 binding was made similar to that proposed by Moore, Huxley & DeRosier (1970) in its appearance. (In Fig.II-6 and hereafter, the actin monomers are numbered differently from in Fig.II-4(a).) Figs.II-7(a) and (b) show $I_{\ell}(R)$ and $\Delta Q(r,z)$ calculated for this model, respectively. In order to improve agreement between calculated $I_{\ell}(R)$ or $\Delta Q(r,z)$ and Fig.II-3(a) or Fig.II-5(a), we introduced troponin molecules to the model, in the way proposed by Ohtsuki (1974) for the thin filament of chicken breast muscle. His proposal implies that the troponin sites have the 2_1 symmetry if the F-actin has 28 subunits in 13 turns. This feature has been recently supported by Wray et al. (1978) and Maéda et al. (1979). In our calculation, these troponin molecules were represented by overlapping spheres as in the case of myosin head. After testing many trial models, however, we found it very difficult to overcome the following discrepancies as far as we assumed that the F peak in Fig.II-5(a) corresponded to the myosin head-myosin head vector. The discrepancies were that the peak appearing at the F position (marked F_a

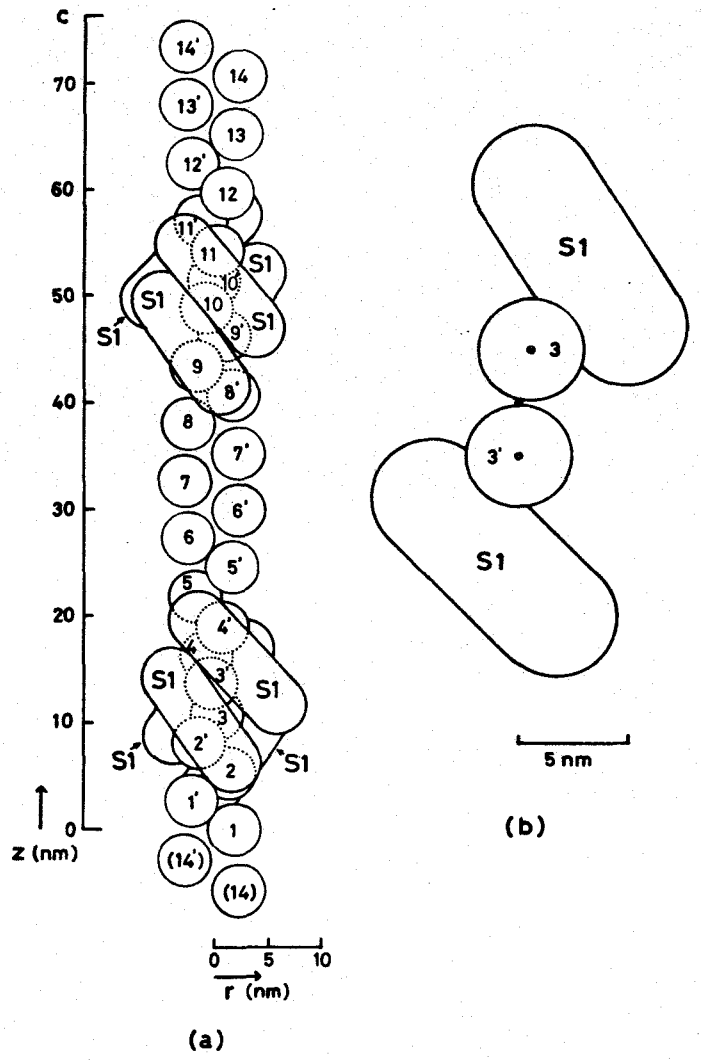

Fig.II-6. An example of the models which were constructed on the assumption that the F peak in Fig.II-5(a) corresponds to the myosin head-myosin head vector. Numbered circle stands for an actin monomer. (a) side view. (b) top view around the 3 and 3' actin monomers. Small solid and open circles denote the z axis and the centre of actin monomers, respectively in (b). The shape of S1 is the same as adopted in the calculation by Miller & Tregear (1972). The way of S1 binding to actin monomers was made similar to that proposed by Moore et al. (1970).

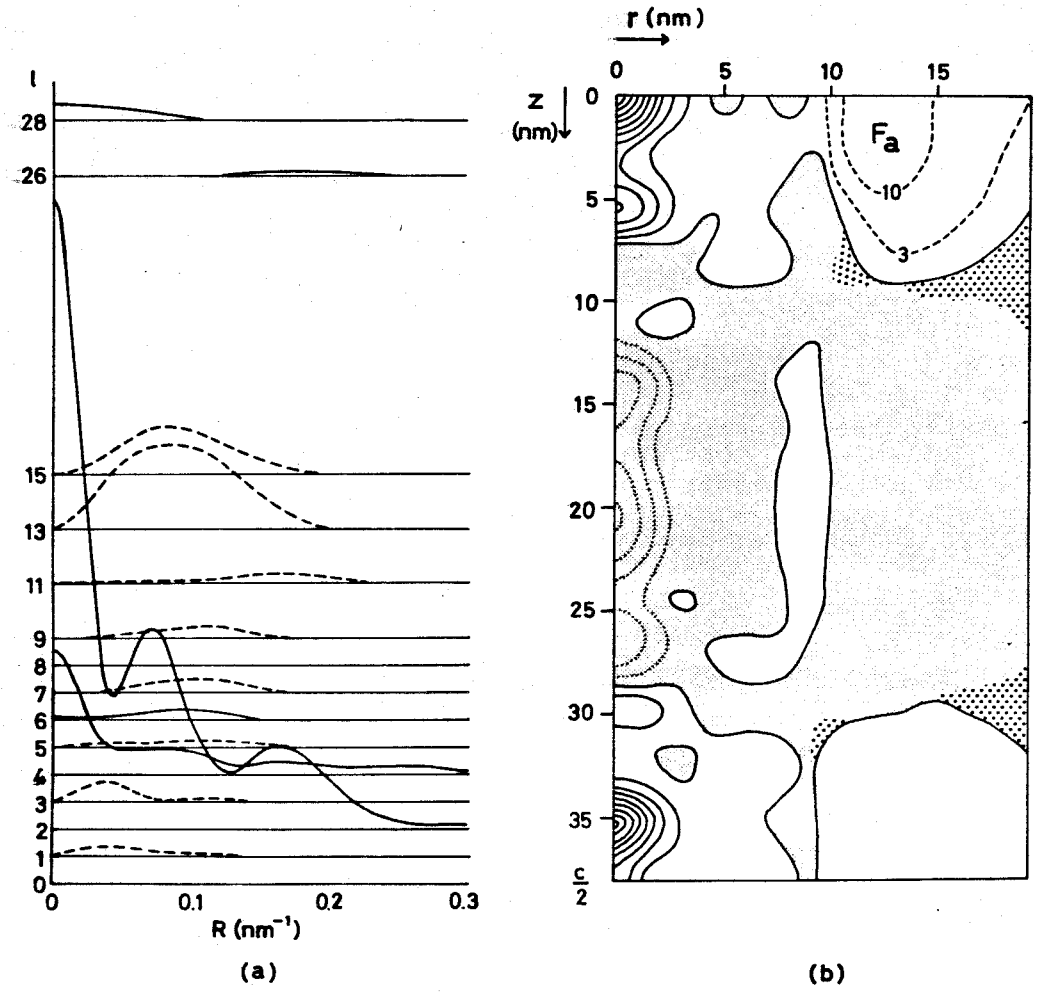

Fig.II-7. $I_\ell(R)$ and contour map of $\Delta Q(r,z)$ calculated for the model in Fig.II-6. (a) $I_\ell(R)$ ($\ell \neq 0$). (b) contour map of $\Delta Q(r,z)$. Contour lines of 3 and 10 are given by dashed line in the region around F_a. Other notations in (a) and (b) are the same as in Figs.II-3 and 4(c), respectively.

in Fig.II-7(b)) was too high (17 compared to 6 of F in Fig.II-5(a)) and that calculated $I_2(R)$ exhibited too narrow meridional peak (compare Fig.II-7(a) to Fig.II-3(a)).

Here we mention that the general feature of Fig.II-5(b) is quite similar to Fig.II-4(c) except for the α and α' peaks. (Note that the normalization factors for the two figures are different.) This fact suggests that the peaks other than α and α' in Fig.II-5(b) are caused by actin-actin vectors and the α and α' peaks can be looked upon as an indication of the existence of other molecules bound to F-actin filament. Also the α peak sits nearly at the same place having nearly the same height (5) as the F Peak (6) in Fig.II-5(a). Therefore, it seemed to be one possibility that the F peak in Fig.II-5(a) corresponds to the vector connecting troponin molecules and that the B shoulder in Fig.II-5(a) corresponds to the vector connecting myosin heads. Then calculations were made postulating these. The r coordinate of centre of gravity of troponin molecules was chosen so as to produce a peak at the F position. Again various models were tested, treating shapes, ways of binding and molecular weights (see below) of myosin heads and troponin molecules as variables. Figs.II-8(a) $\sim$ (c) show one of the models which gave the greatest resemblance between observed and calculated $I_\ell(R)$ and $\Delta Q(r,z)$. The troponin molecule in this model was an elongated rod 4.0nm wide and 9.5nm long along the fibre

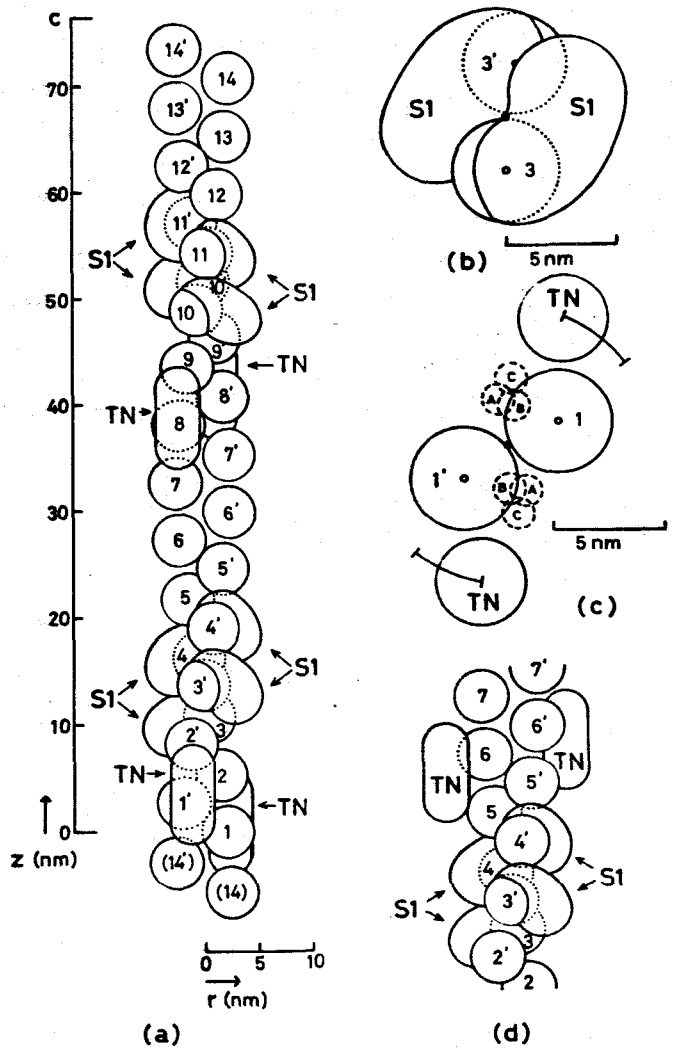

Fig.II-8. Models proposed for the thin filament of crab striated muscle in the rigor state. Numbered circle stands for an actin monomer. TN, troponin molecule. (a) side view of a model. (b) top view of the part around the 3 and 3' actin monomers. (c) top view of the part around the 1 and 1' actin monomers. Arcs show range of uncertainty of the angular coordinate ϕ of TN. Three dashed circles indicate the positions of tropomyosin molecules proposed by Wakabayashi et al. (1975) (A and B), and Spudich et al. (1972) (C). Other notations in (b) and (c) are the same as in Fig.II-6(b). (d) the other possible model.

axis. Figs.II-9(a) and II-10(a) show $I_\ell(R)$ and $\Delta Q(r,z)$ calculated for this model. Figs.II-9(b) and II-10(b) are given to see contributions from troponin and myosin head separately. For these figures we deleted troponin molecules in Figs.II-8(a) ∿ (c) and calculated $I_\ell(R)$ and $\Delta Q(r,z)$ for the rest. The F, F' and E peaks in Fig.II-10(a) are absent in Fig.II-10(b) because they correspond to troponin-troponin and troponin-myosin head vectors, respectively, in our model. Now the peak height of F is 6 in Fig.II-10(a), the same as in Fig.II-5(a). The peaks or shoulders at A, B, B', C, C', D, D' in Fig.II-5(a) are reproduced fairly well in Fig.II-10(b), indicating that they are largely due to myosin heads. The width of the meridional peak of $I_2(R)$ has become large in Fig.II-9(b), and approximately the same as the observation in Fig.II-9(a). It should be noticed that general appearance of Figs.II-3(a) and II-9(b) are similar except for details. This point will be discussed later in connection with Fig.II-14.

The F peak in Fig.II-5(a) sits around r = 13nm and thus the r coordinate of centre of gravity of troponin molecule was put 6.5nm in Fig.II-8, which is smaller than but comparable to 8.0nm suggested by Wray et al. (1978) for lobster (and crayfish) fast muscles. The r coordinate of myosin head is 2.8nm in Fig.II-8. We did not expect such a small value but analysis of the experimental data has forced us to propose it as explained above.

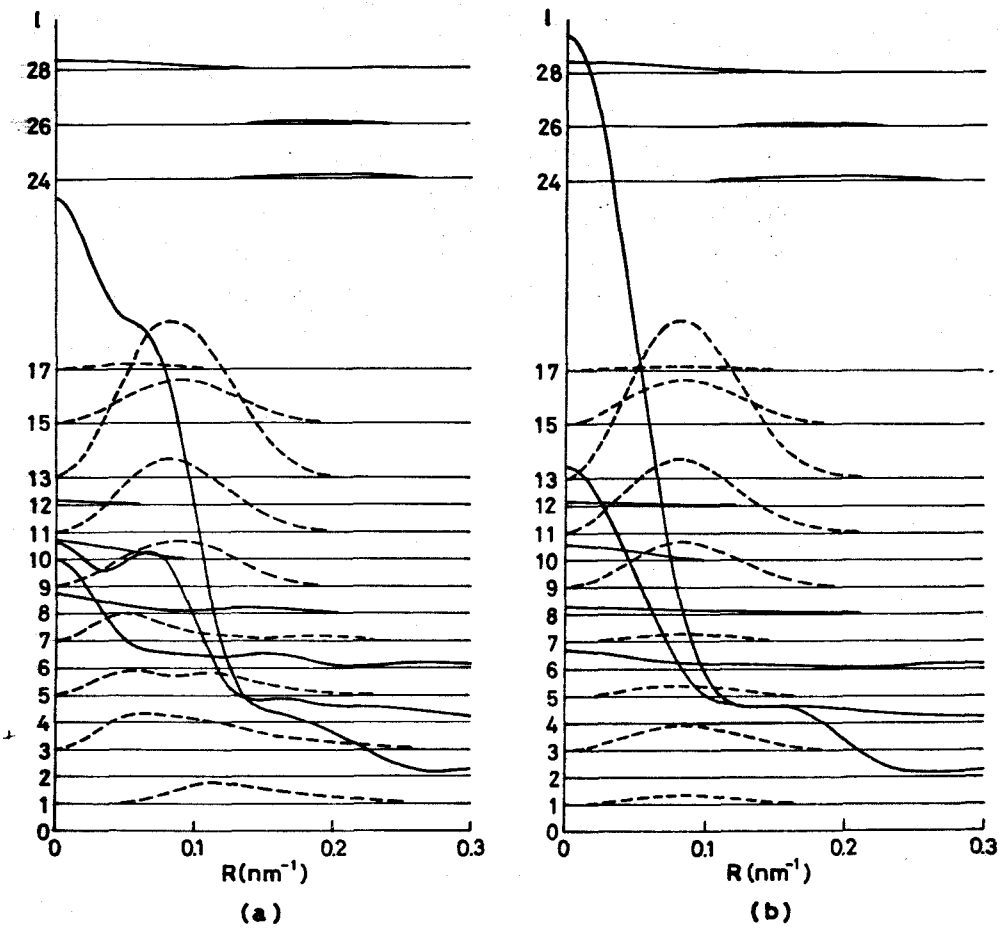

Fig.II-9. Calculated $I_\ell(R)$ ($\ell \neq 0$). Notations are the same as in Fig.II-3. (a) calculated for the model shown in Figs.II-8(a) ∿ (c). $I_\ell(R)$ were scaled so as to give $\sum_\ell I_\ell(R)$ the same value as in Fig.II-3(a). (b) calculated for the model in which the troponin molecules were deleted in Figs.II-8(a) ∿ (c). $I_\ell(R)$ were scaled referring to (a), considering decrease of the total molecular weight.

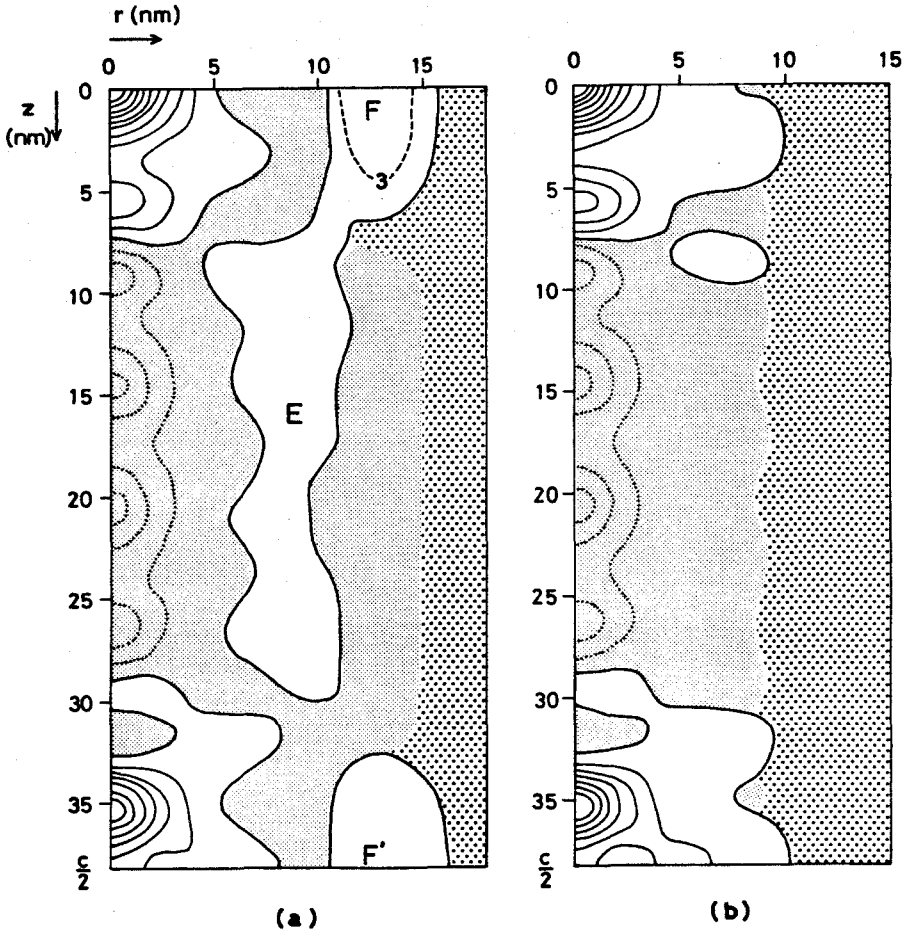

Fig.II-10. Contour map of $\Delta Q(r,z)$. (a) calculated for the model shown in Figs.II-8(a) ∿ (c). Contour line of 3 is given by dashed line in the region around F. (b) calculated for the model in which the troponin molecules were deleted in Figs.II-8(a) ∿ (c). Peak heights at the origins were normalized to 1,000 in both (a) and (b). Other notations are the same as in Fig.II-4(c).

In considering trial models, it was a question how much portion of myosin head is incorporated in the thin filament and contributes to the layer-line diffractions. Therefore, we tested various molecular weights for the bound myosin head. We have assumed that the actin monomer was a sphere of the radius of 2.4nm and had the molecular weight of 42,000 so that its density was 1.20g/cm^3. Values between 50,000 and 350,000 were tested for the molecular weight of bound myosin head assuming the same density as actin, and the best fit was obtained for 100,000 $\sim$ 150,000. These value are close to 110,000 $\sim$ 120,000 reported for one S1 in the rabbit striated muscle (Lowey et al., 1969; Onodera & Yagi, 1971). The molecular weight of troponin was estimated as about 100,000 so as to give the F peak in Fig.II-10(a) the same height as in Fig.II-5(a). This value is close to the molecular weight of troponin in the other crab muscle, 96,000 reported by Maeda et al. (1979).

The structure of tropomyosin has been discussed by several authors (Spudich, Huxley & Finch, 1972; Parry & Squire, 1973; Haselgrove, 1973; Huxley, 1973; Gillis & O'Brien. 1975; Wakabayashi et al., 1975). The proposed positions are depicted by dashed circles in Fig.II-8(c). We examined contributions from tropomyosin to $I_\ell(R)$ and $\Delta Q(r,z)$ based on the models by Parry & Squire (1973) and Haselgrove (1973). Results showed that its contributions

to $I_2(R)$, $I_4(R)$ and $I_6(R)$ are not negligible but small and that they bring about only little effect on $\Delta Q(r,z)$ because of its slender shape. More accurate data seemed to be needed to discuss the structure of tropomyosin.

There has been some uncertainty about the troponin position with regard to ϕ coordinate as was mentioned in our previous report (Namba et al., 1979). The range of ϕ which gives practically the same $I_\ell(R)$ and $\Delta Q(r,z)$ is indicated by arcs in Fig.8(c). It seemed reasonable to expect some spatial contact between the two regulatory proteins, and we set the troponin molecules as close as possible to tropomyosin within this range in Fig.II-8.

Features of the model shown in Figs.II-8(a) ∿ (c) may be summarized as follows.

(1) The S1 are bound to the 3, 3', 4, 4' and 10, 10', 11, 11' actin monomers when the actin monomers are numbered as 1 ∿ 14 along one strand of the long-pitch helix and 1' ∿ 14' along the other, 1' being neighboured by 1 and 2 as shown in Fig.II-8(a).

(2) The centre of gravity of bound S1 sits at r coordinate of about 2.8nm.

(3) The troponin molecules sit with their centres of gravity at roughly the same z coordinates as the 1, 1' and 8, 8' (or 5',6 and 12', 13) actin monomers and at r coordinate of 6.5nm.

(4) The estimated molecular weight of troponin is about

100,000.

The model shown in Figs.II-8(a) ∿ (c) is, however, not a unique solution concerning the position of troponin and there is another model which gives the same order of agreement of $I_\ell(R)$ and $\Delta Q(r,z)$. It was obtained by putting troponin molecules at the places shown in Fig.II-8(d). Centres of gravity of troponin molecules are at roughly the same z coordinates as the 1, 1', 8, 8' actin monomers in Fig.II-8(a) but as the 5', 6, 12', 13 actin monomers in Fig.II-8(d).

In the above we discussed only on the models in which myosin heads bind to the neighbouring actin monomers. We examined also other models. For instance, we calculated $I_\ell(R)$ and $\Delta Q(r,z)$ for the model which was proposed for the insect flight muscle by Offer & Elliott (1978) on the basis of the electron micrographs taken by Reedy (1967, 1968). The model is depicted in Fig.II-11 after the pictures of Figs.2 and 5 of the paper by Offer & Elliott (1978). The S1 bind to the 3, 3', 5, 5' and 10, 10', 12, 12' actin monomers in Fig.II-11(a). We assumed that the molecular weight of S1 was 110,000 and calculated $I_\ell(R)$ and $\Delta Q(r,z)$ for this model. Results are shown in Fig.II-12. Differences between Figs.II-12(a) and II-3(a) and between Figs.II-12(b) and II-5(a) are significant, suggesting that the model in Fig.II-11 does not fit to the thin filament of the crab striated muscle in the rigor state.

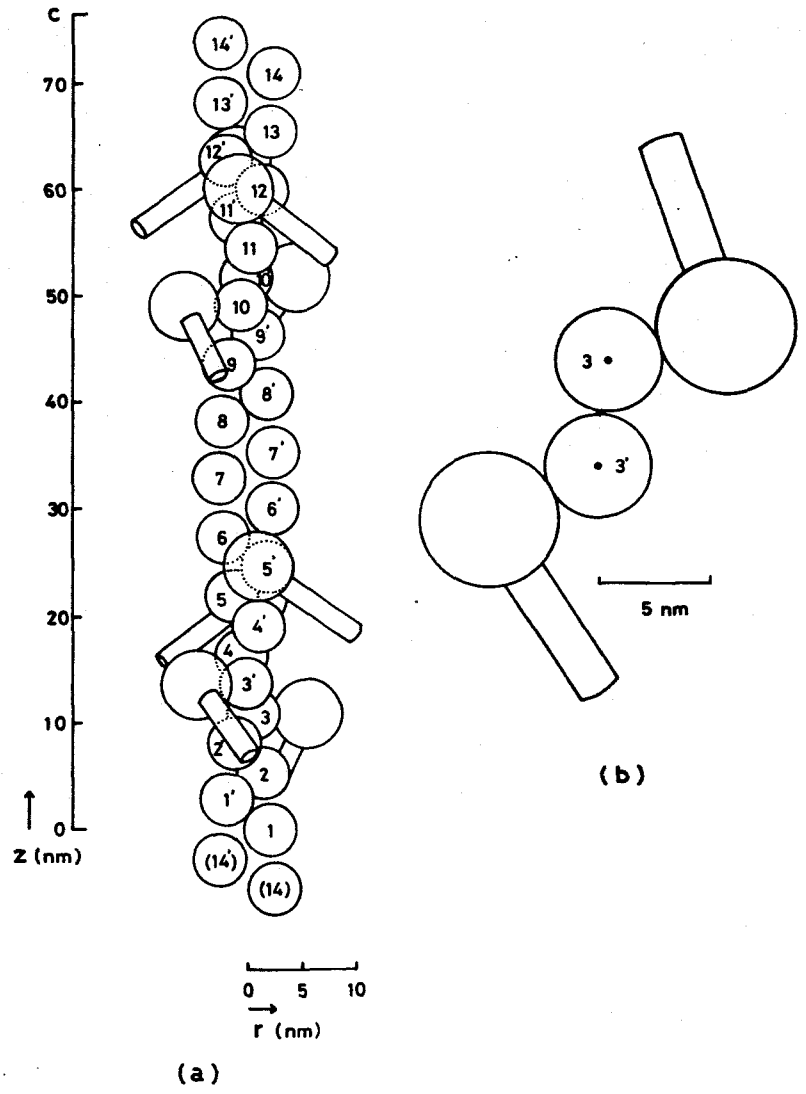

Fig.II-11. A model proposed by Offer & Elliott (1978) for the thin filament of insect flight muscle in the rigor state. Numbered circle stands for an actin monomer; large circle with bar, S1. (a) side view. (b) top view around the 3 and 3' actin monomers. Other notations are the same as in Fig.II-6(b).

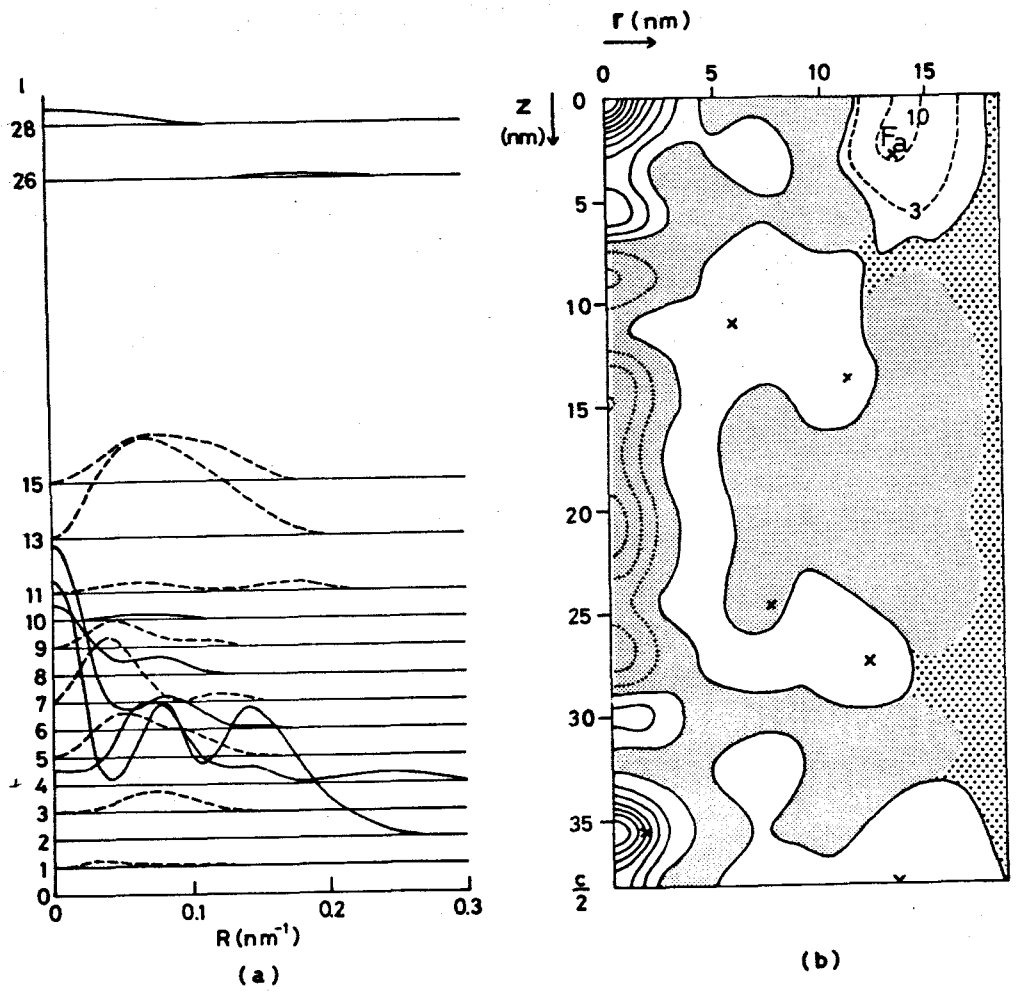

Fig.II-12. $I_\ell(R)$ and $\Delta Q(r,z)$ calculated for the model in Fig.II-11. (a) $I_\ell(R)$ ($\ell \neq 0$), scaled in the same manner as in Fig.II-9(a). (b) contour map of $\Delta Q(r,z)$. Contour lines of 3 and 10 are given by dashed line in the region around F_a. Peak height at F_a is 11. Cross stands for a head of vector connecting centres of gravity of S1 in Fig.II-11. Other notations in (a) and (b) are the same as in Figs.II-3 and 4(c), respectively.

II-5. Discussion

(a) $Q(r,z)$ and $\Delta Q(r,z)$

As is well known, the Patterson function such as $Q(r,z)$ is very useful in structure analysis when its contour map exhibits distinct peaks indicating inter-atomic or inter-molecular vectors (Franklin & Gosling, 1953). The function $\Delta Q(r,z)$ can play a similar role according to the theorem 5. In principle, $Q(r,z)$ contains more information on the structure than $\Delta Q(r,z)$ since $Q(r,z)$ contains the contribution from $I_0(R)$. For practical purposes, however, problems are how to calculate the function from experimental data and how to extract the information of the structure from it. In our studies of the crab muscle, $\Delta Q(r,z)$ could be calculated directly from experimental data by Eq.(II-14) whereas $Q(r,z)$ could not be calculated since $I_0(R)$ was not available experimentally. Naturally, if a structural model is settled, $I_0(R)$ can be calculated from it. Fig.II-13 shows a contour map of $Q(r,z)$, which was calculated for the thin filament in the rigor state, with observed $I_\ell(R)$ of $\ell \neq 0$ in Fig.II-3(a) and $I_0(R)$ calculated with the model in Fig.II-8(a). Peaks appeared more distinctly in Fig.II-5(a) than in Fig.II-13, suggesting that $\Delta Q(r,z)$ would be more useful than $Q(r,z)$ even if $Q(r,z)$ were obtained directly from experimental data. Our studies based on $\Delta Q(r,z)$ had some similarity to the structure analysis by the heavy atom method in crystal structure

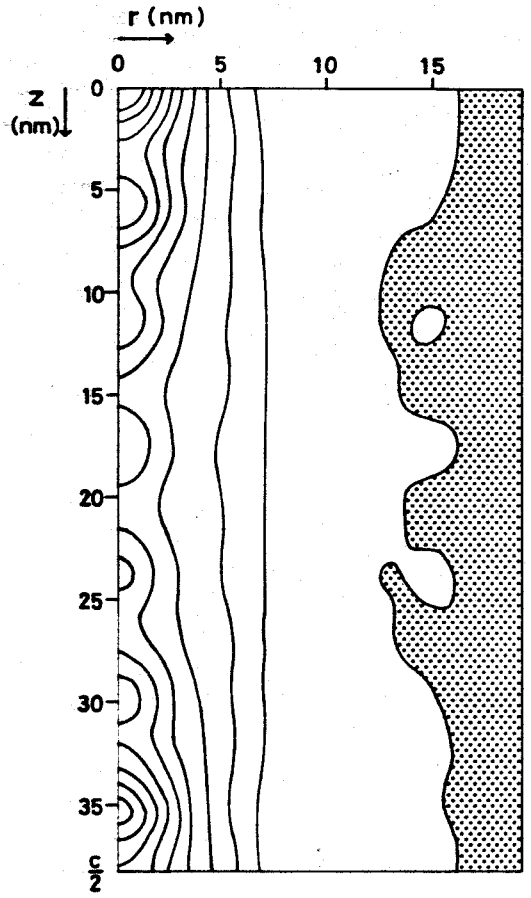

Fig.II-13. Contour map of Q(r,z) calculated for the thin filament in the rigor state, by use of observed $I_{\ell}(R)$ ($\ell \neq 0$) and calculated $I_0(R)$ for the model in Fig.II-8. Notations are the same as in Fig.II-4(b).

analysis. The myosin heads and troponin molecules played the role of heavy atoms on the $\Delta Q(r,z)$ map.

As mentioned in connection with Fig.II-4(c), a contour map of $\Delta Q(r,z)$ gives an outer diameter of the fibre as a boundary between non-zero and zero regions. In Fig.II-5(a), the boundary lay around r = 15nm, so that the outer diameter of the thin filament in the rigor muscle was roughly 15nm. Fig.II-5(b) shows that the r coordinate of the boundary did not change very much on average in the relaxed state. In our scheme, the outer diameter of the thin filament is determined by troponin molecules in both the rigor and relaxed states.

The $\Delta Q(r,z)$ function seems to be a useful mathematical tool in structure analysis of other muscles or more generally of other fibre materials.

(b) $I_\ell(R)$ and $\Delta Q(r,z)$

The function $\Delta Q(r,z)$ can be calculated with $I_\ell(R)$ of $\ell \neq 0$ by Eq.(II-14), and $I_\ell(R)$ of $\ell \neq 0$ from $\Delta Q(r,z)$ by the inverse transformation. Therefore, mathematically $\Delta Q(r,z)$ should contain the same information on the structure as the set of $I_\ell(R)$ of $\ell \neq 0$. For practical purposes, however, the problem is how easily we can read out information on the structure from the functions. In our studies, $\Delta Q(r,z)$ was very helpful in constructing trial models since it is a function in real space and directly

gives suggestions on the inter-molecular vectors visually. $I_{\ell}(R)$ was also helpful, but more mathematical considerations were needed to read out information from $I_{\ell}(R)$ as it is a function in reciprocal space. Recently Barrington Leigh et al. (1977) and Holmes et al. (1979) have pointed out that the ladder-like appearance of X-ray diffraction pattern in the rigor state supports Reedy's idea (1967, 1968) of periodic marking of the thin filament by myosin heads, in the case of insect flight muscle. We did similar considerations on the diffraction pattern from the rigor crab muscle independently. It is reproduced here since it will be of some help to understand in what respects $I_{\ell}(R)$ was useful by itself for us to reach the model in Fig.II-8.

Calculations for various trial models indicated that the intensity distribution $I_{\ell}(R)$ in the rigor state is largely governed by myosin heads as already mentioned in connection with Fig.II-9(b). Therefore, it seemed worthwhile to examine how the diffraction pattern solely due to myosin heads looks like. Fig.II-14 illustrates a procedure of consideration. According to the model in Fig.II-8, the centres of gravity of myosin heads can be given by the intersections (Fig.II-14(a)) of a continuous helix (b) and sets of four planes (c). The helix has the same pitch as the genetic helix of F-actin, C = 5.89nm (b). The sets of four planes have the same seperation as the

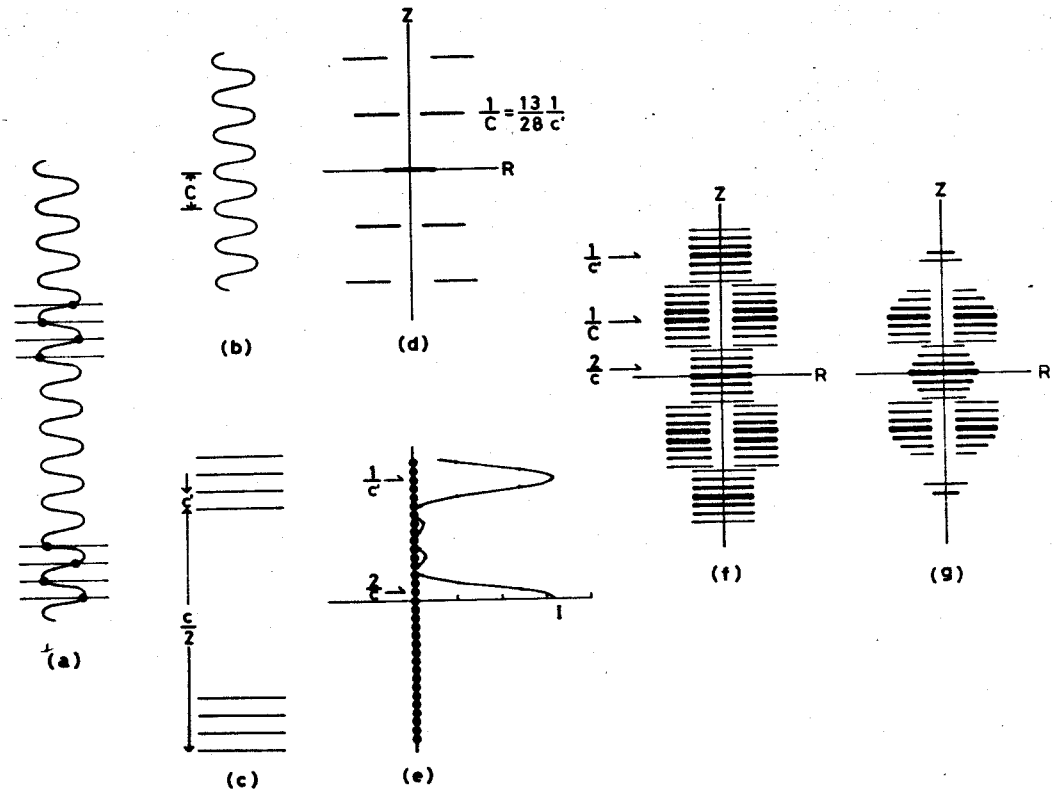

Fig.II-14. Derivation of diffraction pattern solely due to S1 in Fig.II-8. Explanation is given in text. In (f) and (g), thickness of layer line is roughly proportional to the intensity of scattered X-rays.

axial repeat of the actin monomers, c' = 2.73nm (c). The period of the sets is c/2 with c = 76.5nm. Fourier transform of a product of two functions is the convolution of Fourier transforms of the two functions (e.g., Vainshtein, 1966, §1). Fourier transform of the continuous helix is confined on the layer lines at Z = n/C, n = integers, on which Bessel functions J_n determine the scattering intensity (Fig.II-14(d)). Fourier transform of sets of planes is a series of points on the Z axis with the spacing of 2/c (dots in Fig.II-14(e)). The weight of each dot (or δ function) is proportional to Laue function for one set of the four planes (the curve in Fig.II-14(e)). Therefore, if myosin heads in Fig.II-8 are approximated by point scatterers, Fourier transform of them is a convolution of the pattern in Fig.II-14(d) and the series of weighted δ function in Fig.II-14(e), resulting in such a diffraction pattern as shown in Fig.II-14(f). The myosin heads, however, will not be represented well by a point scatterer since it has a large volume. Therefore, Fig.II-14(f) should be further weighted by its squared molecular scattering factor which is expected to have a maximum at the origin and decrease with increasing Z and R coordinates. Resultant diffraction pattern would be such as depicted in Fig.II-14(g). It may be said that general feature of the intensity distribution in Fig.II-1(a) is fairly well reproduced by Fig.II-14(g).

The half width of the curve (Laue function) shown in Fig.II-14(e) is for the two pairs of myosin heads per c/2 in Fig.II-14(a). The width will increase for a single pair and decrease for three pairs. Therefore, the way of decays of $I_2(R)$, $I_4(R)$, $I_6(R)$ on the meridian and of $I_{11}(R)$, $I_9(R)$, $I_7(R)$ on the off-meridian is an indication of how many pairs of myosin heads are bound succesively in c/2 of the thin filament. Wray et al. (1978) suggested that the two or three pairs might be possible. We found good agreement between observed and calculated decays for the two pairs model, supporting the conclusion derived from the $\Delta Q(r,z)$ function.

Variation of $I_\ell(R)$ along the R axis in Fig.II-14(g) depends upon magnitude of the r coordinate of centre of gravity of myosin heads in Fig.II-14(a). Fig.II-15 demonstrates this by giving $I_2(R)$ as a function of R for the models explained in the figure legend. The curves c, d, e, f are for the models which consist of only F-actin and myosin heads. The r coordinates of centres of gravity of myosin heads are, in unit of nm, 2.8 for c, 7.0 for d, 7.4 for e, 10.4 for f. It is apparent that the half width of the meridional peak (the peak near the origin) of $I_2(R)$ decreases with increasing r coordinate. The curve b is for our model in Fig.II-8. Fig.II-15 indicates that large width of the curve b, which is almost the same as that of the observed $I_2(R)$ (the curve a), is caused by relatively

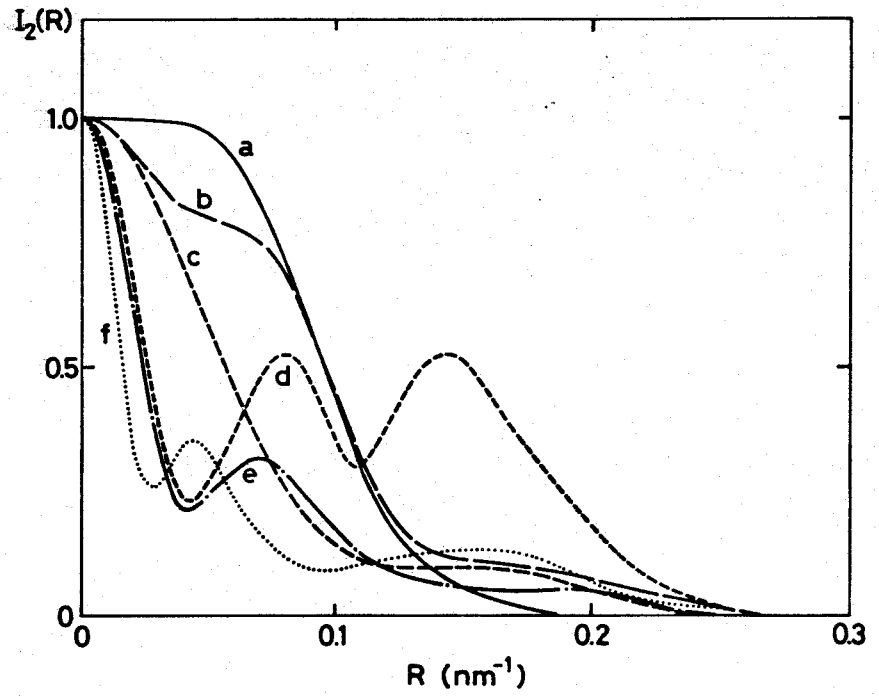

Fig.II-15. $I_2(R)$ calculated for various models in comparison with observation. All curves were normalized to one at R = 0. a, observed; b, calculated for the model in Fig.II-8(a); c, calculated for the model in which the troponin molecules were deleted in Fig.II-8(a); d, calculated for the Offer-Elliott model in Fig.II-11; e, calculated for the model in Fig.II-6; f, calculated for the two-paired Miller-Tregear model described in Section II-4(c).

large width of the curve c in cooperation with the contribution from an off-meridional peak by troponin. Thus the small value of r coordinate of myosin heads seemed to be inevitable to interpret the observed feature of $I_2(R)$.

(c) The model

We have proposed two models for the decorated thin filament as shown in Figs.II-8(a) and (d). Difference between these two models is related with the polarity of the assembly of F-actin and S1 along the z axis. (This polarity is easily recognized by the shape of S1 in Fig.II-8(a) or (d).) The model shown in Fig.II-8(a) has troponin molecules closer to tails of S1, whereas the model in Fig.II-8(d) has troponin molecules closer to heads of S1. A vector connecting centres of gravity of S1 and troponin molecules in Fig.II-8(a) has its mate in Fig.II-8(d) possessing almost the same length and opposite direction. Therefore, the two models gave almost the same $I_\ell(R)$ and $\Delta Q(r,z)$. Common features of these two model are: (1) periodic binding of S1, (2) two pairs of S1 bind to neighbouring actin monomers in half a period of the thin filament, (3) the centre of gravity of S1 has small r coordinate (2.8nm), (4) the centre of gravity of troponin has large r coordinate (6.5nm). Very recently, two structural models have been proposed for the rigor muscles on the basis of X-ray studies: the one is for the lobster

(or crayfish) fast muscles by Wray et al. (1978) and the other is for the insect flight muscle by Holmes et al. (1979). The model of Wray et al. is similar to ours in the features of (1) and (4) but different in (3). They proposed the feature of (2) as a possibility. The model of Holmes et al. is also similar to ours in (1) and (2) but different in (3). Holmes et al. did not take troponin into account in their model. The r coordinate of centre of gravity of S1 was roughly estimated as 8.0nm in Fig.6 of the paper by Wray et al. (1978). The r coordinate is 6.1nm in the model by Holmes et al. They are large compared to our value of 2.8nm. We calculated $I_{\ell}(R)$ and $\Delta Q(r,z)$ for their models and obtained results similar to the case of the model shown in Fig.II-7: the peak heights of the F peak were 2 or 3 times larger than that in Fig.II-5(a) and $I_2(R)$ exhibited too narrow meridional peaks. As described in the preceding section, we started our model construction giving large values to the r coordinate of centre of gravity of S1, but could not reach satisfactory results for the crab striated muscle. Presumably the structures of the insect flight, lobster and crayfish fast muscles are different from that of the crab leg striated muscle in the way of S1 binding.

The estimated molecular weight of bound myosin head, 110,000 ∿ 150,000 was close to the value of S1 for the rabbit striated muscle, 110,000 ∿ 120,000 (Lowey et al.,

1969; Onodera & Yagi, 1971). Presumably almost all part of the binding S1 is incorporated in the thin filament being governed by the structural period of F-actin. The X-ray determined molecular weight of troponin as 100,000 which is comparable to 96,000 in the other crab striated muscle (Maéda et al., 1979) and 88,000 (Perry et al., 1973) or 76,000 ∿ 82,000 (Ebashi, Ohtsuki & Mihashi, 1973) in the rabbit striated muscles. In Fig.II-8(c), troponin sits closer to tropomyosin than in our previous model (Namba et al., 1979). It seems reasonable to expect some spatial contact between two regulatory proteins, and the present model might admit it.

Offer & Elliott (1978) mentioned that the thin filaments sit on special positions of two-fold rotation symmetry in the insect flight muscle and pointed out a possibility that the periodic binding of S1 in Fig.II-11 could be resulted in if the azimuth of S1 binding would be restricted to a very limited angular range by the thick filament. Recently Haselgrove & Reedy (1979) also have discussed on this idea. Wray et al. (1978) did similar considerations on the lobster and crayfish striated muscles. The crab striated muscle, however, has the structure quite different from them (cf. Chapter I; Wakabayashi & Namba, 1978; Maéda et al. 1979): number ratio of the thin filament in the unit cell is 6 : 1 whereas it is 3 : 1 in the above-mentioned muscles, and the thin filament does not

sit on a high symmetry position in the crab muscle. Our models in Fig.II-8 seem to suggest that the troponin molecules determine the sites favorable for binding of S1 on the thin filament in the crab muscle.

(d) On the structure of the thin filament in the relaxed state

In our scheme, a zeroth approximation of the structure of the thin filament in the relaxed state will be obtained by deleting S1 in Fig.II-8. We calculated $I_{\ell}(R)$ and $\Delta Q(r,z)$ for this model. Figs.II-16(a) and (b) have some similarities to Figs.II-3(b) and II-5(b), respectively. We are trying to collect more accurate data for detailed structural studies of relaxed muscles.

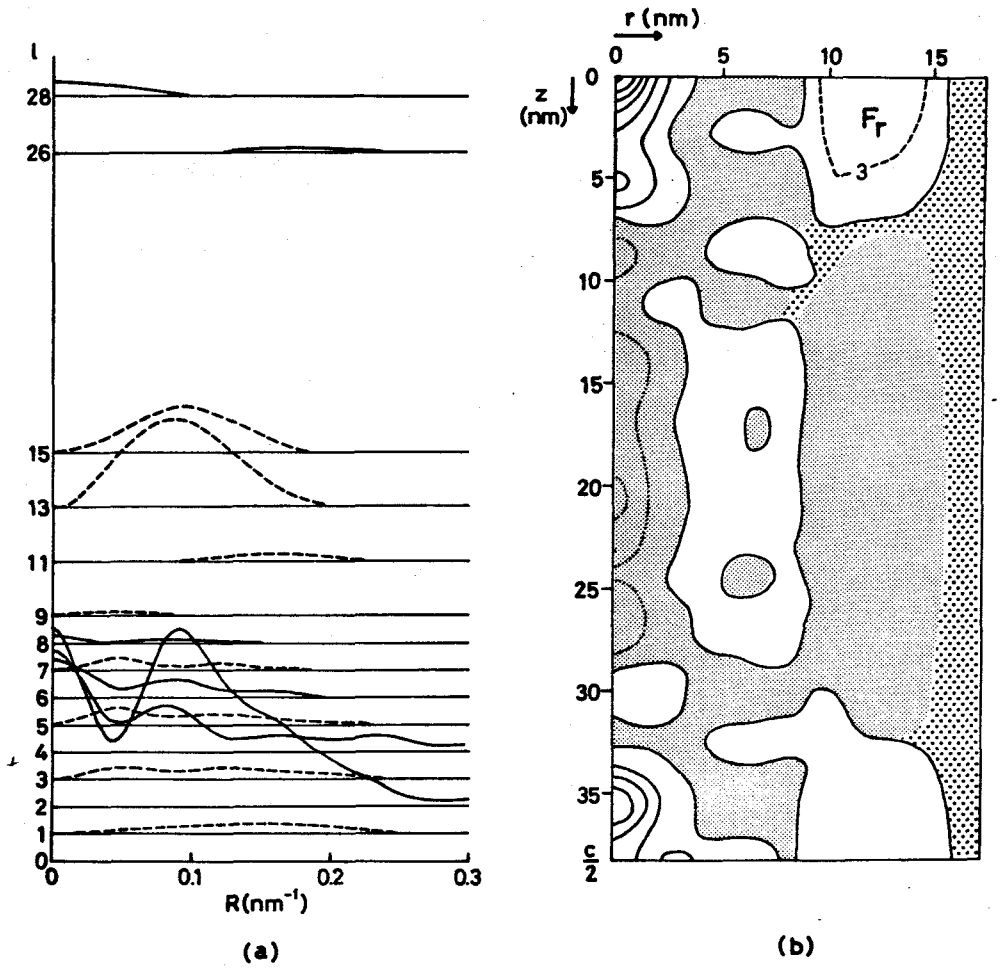

Fig.II-16. $I_\ell(R)$ and contour map of $\Delta Q(r,z)$ calculated for the tentative model of the thin filament in the relaxed state, in which S1 were deleted in Fig.II-8(a). (a) $I_\ell(R)$ ($\ell \neq 0$). $I_\ell(R)$ was scaled in the same manner as in Fig.II-9(b). (b) $\Delta Q(r,z)$. Contour line of 3 is given by dashed line in the region around F_r. Peak height of F_r is 6. Other notations in (a) and (b) are the same as Figs.II-3 and 4(c), respectively.

REFERENCE

April, E. W., Brandt, P. W. & Elliott, G. F. (1971). *J. Cell Biol.* 51, 72-82.

Auber, J. & Couteaux, R. (1963). *J. Microscopie* 2, 309-324.

Barrington Leigh, J., Goody, R. S., Hofmann, W., Holmes, K. C., Mannherz, H. G., Rosenbaum, G. & Tregear, R. T. (1977). In *Insect Flight Muscle* (Tregear, R. T., ed.), pp.137-146, Elsevier North Holland, Amsterdam.

Brenner, S. & Horne, R. W. (1959). *Biochim. Biophys. Acta* 34, 103-110.

Bullard, B., Hammond, K. S. & Luke, B. M. (1977). *J. Mol. Biol.* 115, 417-440.

Ebashi, S. & Endo, M. (1968). *Prog. Biophys. Mol. Biol.* 18, 123-183.

Ebashi, S., Ohtsuki, I. & Mihashi, K. (1973). *Cold Spring Harbor Symp. Quant. Biol.* 37, 215-223.

Elliott, G. F., Lowy, J. & Worthington, C. R. (1963). *J. Mol. Biol.* 6, 295-305.

Elliott, G. F., Lowy, J. & Millman, B. M. (1967). *J. Mol. Biol.* 25, 31-45.

Franklin, R. E. & Gosling, R. G. (1953). *Acta Crystallogr.* 6, 678-685.

Gillis, J. M. & O'Brien, E. J. (1975). *J. Mol. Biol.* 99, 445-459.

Goody, R. S., Holmes, K. C., Mannherz, H. G., Barrington Leigh, J. & Rosenbaum, G. (1976). *Biophys. J.* 15, 687-705.

Hardwicke, P. M. D. & Hanson, J. (1971). *J. Mol. Biol.* 59, 509-516.

Haselgrove, J. C. (1973). *Cold Spring Harbor Symp. Quant. Biol.* 37, 341-351.

Haselgrove, J., Stewart, M. & Huxley, H. E. (1976). *Nature* 261, 606-608.

Haselgrove, J. C. & Reedy, M. K. (1979). *Biophys. J.* 24, 713-728.

Holmes, K. C., Tregear, R. T. & Barrington Leigh, J. (1979). to be published in *Proc. Roy. Soc. London* (Manuscript supplied to us).

Huxley, A. F. & Niedergerke, R. (1954). *Nature (London)* 173, 973-976.

Huxley, A. F. (1957). *Prog. Biophys. Biophys. Chem.* 7, 255-318.

Huxley, A. F. (1971). *Proc. Roy. Soc.* B178, 1-27.

Huxley, A. F. & Simmons, R. M. (1972). *Nature* 233, 533-538.

Huxley, H. E. & Hanson, J. (1954). *Nature (London)* 173, 973-976.

Huxley, H. E. (1960). In *The Cell* (Brachet, J. & Mirsky, A. E., eds.) vol.4, pp.365-481, Academic Press, New York and London.

Huxley, H. E. & Brown, W. (1967). *J. Mol. Biol.* 30, 383-434.

Huxley, H. E. (1968). *J. Mol. Biol.* 37, 507-520.

Huxley, H. E. (1969). *Science* 164, 1356-1366.

Huxley, H. E. (1971). *Proc. Roy. Soc.* B178, 138-149.

Huxley, H. E. (1973). *Cold Spring Harbor Symp. Quant. Biol.* 37, 361-376.

Klug, A., Crick, F. H. C. & Wyckoff, H. W. (1958). *Acta Crystallogr.* 11, 199-213.

Lowey, S., Slayter, H. S., Weeds, A. G. & Baker, H. (1969). *J. Mol. Biol.* 42, 1-29.

Lowy, J. & Hanson, J. (1962). *Physiol. Rev.* 42, 34-47.

Lowy, J., Millman, B. M. & Hanson, J. (1963). *Proc. Roy. Soc.* B160, 525-536.

Maéda, Y. (1978). *Eur. J. Biochem.* 56, 547-556.

Maéda, Y. (1979). *Nature (London)* 277, 671-672.

Maéda, Y., Matsubara, I. & Yagi, N. (1979). *J. Mol. Biol.* 127, 191-201.

McGillavry, C. H. & Bruins, E. M. (1948). *Acta Crystallogr.* 1, 156-158.

Miller, A. & Tregear, R. T. (1972). *J. Mol. Biol.* 70, 85-104.

Millman, B. M. & Bennett, P. M. (1976). *J. Mol. Biol.* 103, 439-467.

Moore, P. B., Huxley, H. E. & DeRosier, D. J. (1970). *J. Mol. Biol.* 50, 279-295.

Namba, K., Wakabayashi, K. & Mitsui, T. (1979). In *Cross-Bridge Mechanism in Muscle Contraction* (Sugi, H. & Pollack, G. H., eds.), pp.445-456, University of Tokyo Press, Tokyo, and *J. Mol. Biol.* in press.

Offer, G. & Elliott, A. (1978). *Nature (London)* 271, 325-329.

Ohtsuki, I. (1974). *J. Biochem.* (*Tokyo*) 75, 753-756.

Onodera, M. & Yagi, K. (1971). *J. Biochem.* (*Tokyo*) 69, 145-153.

Oster, G. & Riley, D. P. (1952). *Acta Crystallogr.* 5, 1-6.

Parry, D. A. D. & Squire, J. M. (1973). *J. Mol. Biol.* 75, 33-55.

Perry, S. V., Cole, H. A., Head, J. F. & Wilson, F. J. (1973). *Cold Spring Harbor Symp. Quant. Biol.* 37, 251-262.

Podolsky, R. J., Nolan, A. C. & Zaveler, Z. A. (1969). *Proc. Natl. Acad. Sci.* USA 64, 504-511.

Reedy, M. K. (1967). *Amer. Zool.* 7, 465-481.

Reedy, M. K. (1968). *J. Mol. Biol.* 31, 155-176.

Spudich, J. A., Huxley, H. E. & Finch, J. T. (1972). *J. Mol. Biol.* 72, 619-632.

Szent-Györgyi, A. (1951). In *Chemistry of Muscular Contraction*, 2nd edn. Academic Press, London.

Szent-Györgyi, A. G., Cohen, C. & Kendrick-Jones, J. (1971). *J. Mol. Biol.* 56, 239-258.

Taylor, E. W. (1972). *Ann. Rev. Biochem.* 41, 577-616.

Tonomura, Y. (1972). In *Muscle Proteins, Muscle Contraction and Cation Transport*, University of Tokyo Press, Tokyo.

Tregear, R. T., Milch, J. R., Goody, R. S., Holmes, K. C. & Rodger, C. D. (1979). In *Cross-Bridge Mechanism in Muscle Contraction* (Sugi, H. & Pollack, G. H., eds.), pp.407-421, University of Tokyo Press, Tokyo.

Vainshtein, B. K. (1963). In *Diffraction of X-Rays by Chain Molecules*, Elsevier Publishing Company, Amsterdam, London & New York.

Wakabayashi, K. & Namba, K. (1978). *Proc. Sixth Int. Biophys. Congr. Kyoto, Abstr.* VIII-3-(J), p.381.

Wakabayashi, T., Huxley, H. E., Amos, L. A. & Klug, A. (1975). *J. Mol. Biol.* 93, 477-497.

Wray, J. S., Vibert, P. J. & Cohen, C. (1974). *J. Mol. Biol.* 88, 343-348.

Wray, J. S., Vibert, P. J. & Cohen, C. (1975). *Nature (London)* 257, 561-564.

Wray, J. S., Vibert, P. J. & Cohen, C. (1978). *J. Mol. Biol.* 124, 501-521.

Wray, J. S. (1979). *Nature (London)* 277, 37-40.

Yagi, N. & Matsubara, I. (1977). *J. Mol. Biol.* 117, 797-803.

Yanagida, T., Taniguchi, M. & Oosawa, F. (1974). *J. Mol. Biol.* 90, 509-522.